Nuclear Inst. and Methods in Physics Research, A 878 (2018) 141–158

Contents lists available at ScienceDirect

Nuclear Inst. and Methods in Physics Research, A

journal homepage: www.elsevier.com/locate/nima

Diffraction in neutron imaging—A review

Robin Woracek [a], Javier Santisteban [b], Anna Fedrigo [a], Markus Strobl [a,c,d,*]

[a] European Spallation Source ERIC, Tunavägen 24, 22100 Lund, Sweden
[b] Centro Atómico Bariloche, San Carlos de Bariloche, Rio Negro, Argentina
[c] Paul-Scherrer Institute, 5232 Villigen, Switzerland
[d] Niels-Bohr Institute, University of Copenhagen, Denmark

ARTICLE INFO

Keywords:
Neutron imaging
Neuron transmission
Neutron scattering
Diffraction
Crystallography

ABSTRACT

Neutron imaging is a highly successful experimental technique ever since adequate neutron sources were available. In general, neutron imaging is performed with a wide wavelength spectrum for best flux conditions in transmission geometry. Neutrons provide outstanding features in the penetration of many structural materials, which often makes them more suited for bulk sample studies than other forms of radiation, often in particular as they are also highly sensitive to some light elements, especially Hydrogen. In contrast to neutron scattering applications, imaging resolves macroscopic structures, nowadays down to, in the best case, below 10 micrometre, directly in real space. However, since more than a decade there is a growing number of techniques and applications in neutron imaging that – supported by powerful neutron sources – are taking advantage of wavelength resolved measurements. In this review we summarize and discuss this outstanding development and how wavelength resolved transmission neutron imaging is successfully exploiting diffraction mechanisms to access crystal structure information in the Angstrom regime, which conventionally is probed in reciprocal space by diffraction techniques. In particular the combination of information gained in real space and on crystallographic length scales makes this neutron imaging technique a valuable tool for a wide range of new applications, while it also qualifies neutron imaging to fully profit from the new generation of powerful pulsed neutron sources.

© 2017 Elsevier B.V. All rights reserved.

Contents

* Corresponding author at: European Spallation Source ERIC, Tunavägen 24, 22100 Lund, Sweden.
E-mail address: markus.strobl@psi.ch (M. Strobl).

http://dx.doi.org/10.1016/j.nima.2017.07.040
Received 30 April 2017; Received in revised form 4 July 2017; Accepted 20 July 2017
Available online 10 August 2017
0168-9002/© 2017 Elsevier B.V. All rights reserved.

1. Introduction

Neutron imaging is generally considered a separate, and at best complimentary, tool to neutron scattering. In contrast to the latter, neutron imaging directly probes samples in real space and on macroscopic length scales ranging from micrometres to decimetres. Neutron scattering, on the other hand, generally targets material structures and dynamics in reciprocal space whilst taking advantage of cold and thermal neutron wavelengths and energies being of the order of hence resolvable interatomic distances and excitation energies.

The main distinction between neutron imaging and its reciprocal space counter parts is, however, that imaging resolves individual structures in real space, while scattering methods average structural features, generally over significant volumes that are exposed to the measured neutron beam. Another significant difference lies in the measurement geometry, which underlines the foci on different signals to be recorded. While the name scattering already implies that the focus is on recording scattered radiation deviating from the incident beam direction, neutron imaging concentrates in general on the transmitted intensity. Consequently, while scattering measurements are angular dispersive with detectors around the sample, in imaging the detector is normally placed in line with the incoming beam downstream the sample position.

However, besides the absorption contributing to the attenuation of the beam by the sample, the transmitted signal also carries the significant signature of scattering, as it is to a first approximation a measure of the position dependent total cross section of the transmitted material as described by Beer–Lambert's law:

$$I(x,y) = I_0(x,y)\, e^{-\int_0^t \Sigma(x,y,z)\cdot \partial z}. \tag{1}$$

Here, $I_0(x,y)$ is the intensity of the incident beam and $I(x,y)$ is the intensity that is detected with spatial resolution in the (x,y) plane of the detector, while $\Sigma(x,y,z)$ is the linear attenuation coefficient distribution in the sample which is integrated along the beam direction z over the sample thickness t. The linear attenuation coefficient itself is defined by the particle density N and the total microscopic cross section $\sigma = \sigma_a + \sigma_s$ with σ_a and σ_s being the microscopic absorption and scattering cross section, respectively, as

$$\Sigma = N\sigma. \tag{2}$$

Although for many materials the scattering cross section is significant or even dominating the attenuation signal, these contributions cannot be distinguished using conventional white beam imaging (a term that refers to using a broad wavelength spectrum over several Angstrom). While using a broad spectrum instead of a well-defined wavelength provides superior flux conditions, it does not allow any extraction of quantitative information concerning the scattering component in conventional neutron imaging.

It was in the wake of the new millennium when digital detectors and continuously improving instruments, resolution and flux conditions paved the way for neutron imaging to evolve from a rudimentary non-destructive testing method to a scientifically advanced characterization tool. Subsequently, due to overlaps in science and applications, instrumental approaches of neutron scattering techniques have moved into the focus of neutron imaging and a range of novel methodical developments was initiated that led to increasing overlap of imaging and elastic scattering techniques. Consequently, neutron imaging is now routinely applied to various scientific questions and regarded as a valuable technique in material science complementing other scattering instrumentation at large scale neutron sources.

Within this review, Section 2 provides some general background on the diffraction mechanisms that are fundamental to the contrast observed in transmission, it addresses instrumental requirements and summarizes various experimental approaches. At the end of Section 2, we attempt, based on this introduction and overview, to implement a terminology that can help the still evolving field to be concise in communication and dissemination. In Section 3, the potential and approaches of diffraction contrast imaging for the characterization of different crystalline features, including strains, phase distributions and microstructural parameters, are introduced and used for discussions and explanations of relevant methodological details, while highlighting the state-of-the-art for respective applications. An overview of applications in different fields, and examples of such are presented in Section 4, based on published results from various research groups. Finally, we provide a short summary with an outlook in Section 5.

2. Diffraction in imaging

2.1. Cross section and Bragg scattering

While the scattering cross section consists of various contributions including coherent and incoherent as well as elastic and inelastic parts, diffraction is focusing on the coherent elastic cross section. Coherent elastic scattering at crystal lattices is described by the Bragg equation [1,2],

$$n\lambda = 2d_{hkl}\sin\theta, \tag{3}$$

where $n = 1, 2, 3, \ldots$, $\lambda = 2\pi/k$ is the neutron wavelength, with k being the modulus of the wavevector, d_{hkl} is the specific crystal lattice distance for the Miller indices h, k, l and θ is the Bragg angle (half of the scattering angle). Correspondingly, diffraction measurements are performed with wavelength and angular resolution in order to retrieve the crystal lattice parameters. The powder diffraction pattern [3,4] of an isotropic polycrystalline material can be described by the coherent elastic differential cross section

$$\frac{\partial\sigma^{el}_{coh}}{\partial\Omega}(\lambda) = \frac{(2\pi)^3 N}{V_0}\sum_{hkl}\delta\left(1 - \frac{2d_{hkl}}{\lambda}\sin\theta\right)|F_{hkl}|^2. \tag{4}$$

Here, $\partial\Omega$ is the solid angle increment, V_0 is the unit cell volume, δ denotes the Dirac delta function, while F_{hkl} is the structure factor for scattering at specific lattice planes. Note that we here use a simplified version of the equation in a scalar form. While for scattering at a crystal, vectors describing the lattice and the incoming and diffracted neutrons in space have to be used, for an isotropic powder there is a rotation symmetry around the incoming neutron wavevector (Debye Scherrer rings), which allows for a scalar notation based on the scalar Bragg equation. For most powder diffraction instruments the detector coverage is therefore mainly in a plane around the sample. Furthermore, it has to also be underlined, that in addition to the parameters in Eq. (4), the analyses of measured data must account for a number of other factors like multiplicity, extinction, Debye–Waller factor and the contribution of interactions other than coherent elastic scattering [5,6].

Neutron imaging measurements in transmission geometry are however not angular dispersive and hence only the integral coherent elastic cross section is relevant, while most of the information about the specific

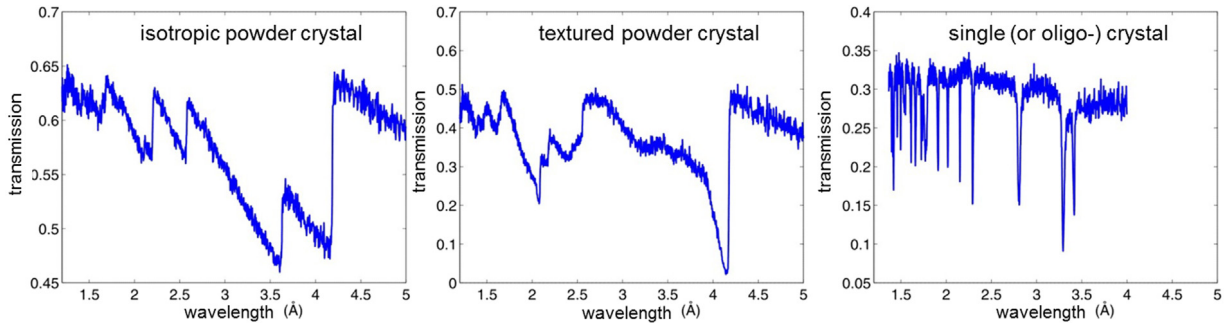

Fig. 1. Attenuation spectra measured in individual pixels in transmission imaging. (a) Transmission of an isotropic powder-like Cu poly-crystal as described in the coherent elastic cross section in Eq. (5). (b) Transmission spectrum of a textured Cu poly-crystal and (c) of a Cu single, displaying inverse individual diffraction peaks, each one corresponding to a diffracted beam in 4π.

scattering angles (2θ) is largely lost. For an isotropic powder-like sample the total coherent elastic cross section can be written as [7,8]

$$\sigma_{coh}^{el}(\lambda) = \frac{\lambda^2}{4V_0} \sum_{hkl}^{2d_{hkl}<\lambda} |F_{hkl}|^2 d_{hkl} \tag{5}$$

where the sum runs over all crystal reflections with interplanar distances d_{hkl} smaller than half the neutron wavelength. So whilst a diffraction instrument with large angular coverage measures Debye Scherrer rings according to the different hkl, a transmission spectrum displays a sawtooth-like pattern as observed in Fig. 1(a). These so-called *Bragg edges* occur because for specific crystal lattice planes characterized by d_{hkl}, the Bragg angle increases as the wavelength increases as $\lambda = 2d_{hkl}$ sin θ until 2θ is equal to 180°. At wavelengths greater than $2d_{hkl}$ no Bragg reflection for this particular d_{hkl} can occur, resulting in a drop in the total cross section, i.e., a sharp increase in the transmitted intensity. While the position of the Bragg edge with respect to the wavelength provides a direct measure of $2d_{hkl}$, the height of the specific Bragg edge gives a direct measure of the number of crystallites having their respective planes oriented normal to the incoming beam.

Eq. (5) is valid not only for powders but also for perfectly random crystallite agglomerates such as metals, ceramics, rocks, etc. However, in many objects some crystallite directions appear much more frequently than others and the material is said to be textured. In such cases, the shape of the transmission spectrum departs from Eq. (5), and some Bragg edges may even be absent, as observed in Fig. 1(b) for the Bragg edge expected near 3.5 Å. Hence, the shape of the total cross section then depends on the orientation distribution function (ODF) of the crystallites composing the object, which is normally quantified by the measurement of pole figures in a powder diffractometer [9]. The transmitted spectrum for textured samples therefore depends on the sample orientation (Ψ) traversed by the neutron beam [10]

$$\sigma_{coh}^{el}(\lambda) = \frac{\lambda^2}{4V_0} \sum_{hkl}^{2d_{hkl}<\lambda} |F_{hkl}|^2 d_{hkl} R\left(\psi, \lambda, d_{hkl}\right) \tag{6}$$

where the factor R is given by a line integral around a circle in the hkl pole figure centred in the direction Ψ of the specimen. In addition, for large grained materials there can be coherent attenuation of the neutron beam within a grain, and the scattered neutron wave results from the interference of the incident and reflected beam process. This phenomenon is called *extinction*, and it has been analysed by Weiss for wavelength resolved neutron transmission in powders in [11]. The model uses the concepts developed for diffraction and assumes that each grain is composed by slightly misaligned (<1°) mosaic blocks, providing an expression that includes all these parameters, but it has not been used by other researchers so far. Extinction becomes particularly important for Bragg edges found at longer wavelengths (>3 Å).

In the extreme case when the specimen is composed of only one crystal, or a small number of crystals (oligo-crystal), the wavelength-dispersive neutron transmission contains a series of dips in intensity appearing at specific neutron wavelengths due to reflection at individual crystallographic planes of individual grains with specific orientation. The position, depth and width of those dips depend on the neutronic properties of the material, like the degree of perfection of the single crystal, and the orientation of the specimen in the neutron beam. In this case, an effective elastic coherent total cross section is given by a sum of peaks (one for each hkl reflection) at wavelengths $\lambda_{hkl} = 2d_{hkl} \sin\theta_{hkl}$ [12] for the individual grains

$$\sigma_{coh}^{el}(\lambda) = \sum_{hkl} y_{hkl} \frac{|F_{hkl}|^2 \lambda_{hkl}^4}{2V_0 \sin^2\theta_{hkl}} P\left(\lambda_{hkl}, \varpi_{hkl}, \lambda\right) \tag{7}$$

where y_{hkl} is an extinction factor, and $P\left(\lambda_{hkl}, \varpi_{hkl}, \lambda\right)$ describes the actual peak shape related e.g. to the mosaicity of the crystal grain. Note, however, that the peak shape as well as the Bragg edges measured for a powder indeed always also depend on the instrument, and in particular the resolution function of a specific instrument.

The consequences of the difference between angular resolved diffraction and spatially resolved imaging are manifold. Powder diffraction patterns can be reduced by integrating over the Debye Scherrer cones to $I(\lambda, \theta)$ and via the Bragg equation to $I(\theta)$ or $I(d)$. Diffraction patterns and curves provide information integral over the effective beam size, i.e. the gauge volume defined by incoming and outgoing collimation. In transmission, however, the imaging geometry enables to measure spatially resolved attenuation spectra, i.e. independent cross section measurements for the points in an image defined by the spatial resolution capability of the set-up.

However, the spectra are integrals along the trajectories of the beam through the sample. Due to the lost angular information the detailed interpretation for single crystals and textured samples becomes very difficult. However, on the other hand spatial variations in texture and crystalline phase across the field of view (FoV) are straightforwardly detected. The implications of the nature of the transmission spectra for different measurements and applications will be discussed in great detail in the next section.

Yet another difference between measurements in diffraction and transmission imaging geometry is a principle difference in signal to background. While in diffraction intensities are measured against a relatively low background, in transmission potentially weak diffraction effects cannot always be resolved against the background of the direct transmitted beam. This limits the applicability of transmission measurements to strongly scattering samples. Nevertheless, for some highly important crystalline materials, like engineering materials such as the metals Fe, Al, Ni, the coherent elastic scattering cross section is dominating the total cross section in the applied wavelength range of Angstroms, which match the interatomic distances of the crystal lattices. Here lies the potential of spatially resolved transmission measurements in observing structural features and transitions in potentially complex geometries and conditions, which imply significant spatial variations of parameters. Particularly under in-situ conditions – but also when high spatial resolution is required – scanning approaches in diffractometers often fail to provide the required insights. However, in many cases for

the above outlined reasons, only the combination of both techniques, which by all means is feasible (compare Fig. 1A(a) and C(a)), might enable to acquire full quantitative understanding. Correspondingly, there have also been a few approaches reported where imaging is conducted in the diffracted rather than in the transmitted beam geometry. A discussion of such approaches is included in the section about various experimental approaches below.

2.2. Wavelength resolution and transmission imaging geometry

A precondition for spatial resolved studies of crystalline characteristics of samples was the introduction of wavelength resolution in neutron imaging. While in principle transmission studies that record the wavelength dependent spectrum through crystalline samples have a long history [6,8,11,13–21], neutron imaging was conventionally conducted using the full available thermal spectrum prohibiting the resolution of the wavelength dependent coherent elastic cross section. It was only in this millennium, that wavelength resolved transmission imaging was applied for spatially resolved studies of crystalline features or based on their wavelength dependent contrast behaviour. Nearly simultaneously corresponding experiments were reported by a neutron imaging group using continuous sources and a diffraction group at the pulsed spallation neutron source ISIS. While the earlier employed an imaging detector with then state of the art spatial resolution of around 100 μm but a poor wavelength resolution of some 10% achieved by a velocity selector [22,23] the latter exploited a time-of-flight (ToF) wavelength resolution of <1% at a diffractometer but poor spatial resolution of a pixelated detector with 2 mm pixel size [21,24–28]. The gap between highly qualitative contrast studies with good spatial resolution at continuous sources [29] and more quantitative studies of crystalline features with poor spatial resolution at pulsed sources [5,25,26,30,31] could only be closed with the introduction of double crystal monochromators [32] at continuous sources and ToF imaging detectors [33–35] at pulsed sources.

2.3. Specific instrumentation

The precondition for achieving spatial resolution with a reasonable FoV with neutrons is a suitable beam geometry and divergence. Due to the fact that suitable optics for imaging with neutrons are not available (yet), dedicated neutron imaging instruments utilize a simple pinhole geometry with a long flight path L and short sample to detector distances l to achieve a significant FoV up to some tens of cm and image resolutions down to few tens of micrometres [36]. In general, the beam divergence in the pinhole with diameter D (on the order of centimetres) is intended to be large in order to achieve a large FoV at the sample position at a distance L (on the order of several metres) from the pinhole. This way the local divergence in a point of the object is small (D/L) and hence provides high spatial resolution $d/2 = lD/(2L)$ capabilities at short sample to detector distances l with suitable imaging detectors [37]. For beams of low divergence and relatively small size, like typically available at diffractometers, imaging experiments on small samples with limited spatial resolution can be performed straightforwardly.

Means for monochromatisation and wavelength resolution in continuous source instruments for imaging are best placed upstream of the pinhole in order not to influence the spatial resolution capability and beam homogeneity. These can be turbine-type velocity selectors [23], crystal monochromators [32] or chopper systems [38,39]. It has to be noted, however, that all these devices viewed through the pinhole introduce spectral inhomogeneities on the FoV [39–44]. The choice between such devices has to be based on the requirements of a specific measurement. The identification and quantification of some crystalline phases for example might only require a loose wavelength resolution of a few percent, while the accurate measurement of residual strains typically requires resolutions around and below one percent (whereas applied strains can be measured in-situ with lower resolutions again [44]). While strain might be deduced from an accurate sampling of a single edge on a very narrow bandwidth, the identification of several phases might require a broad bandwidth. Then again, the quantification of a phase fraction or its 3D distribution can be investigated with one or two discrete wavelengths alone. The best state-of-the-art velocity selectors provide wavelength resolutions down to about 5%, while the currently applied crystal monochromator devices provide wavelength dependent resolutions around 3%. Tailoring the resolution to the needs of a measurement is key for the efficiency of a measurement [45], because the flux, in general, scales with the resolution (better resolution implies lower flux). This is equally true in the space as in the wavelength, i.e. energy, domain. Here sophisticated chopper systems provide significant advantages as they allow tailoring the wavelength resolution to the requirements [39,45–48]. The drawback is on the other hand the need for a ToF imaging detector, which do not yet provide the size of FoV and the spatial resolution achievable with time integrating imaging detectors [37].

At pulsed neutron sources the ToF approach, again requiring suitable ToF detectors, is intrinsically given without further sacrifices in flux. However, at existing short pulse sources, in general, the flux versus resolution is set by the choice of moderator and length of the instrument, and hence cannot be tailored to the requirements of a measurement. Also, the spectral width is largely fixed and cannot be tailored to the needs (except with source pulse suppression enabled by some instruments), and it can, even with the initial choice of instrument length, only be traded against flux and resolution. This situation is somewhat improved at a long pulse source like the European Spallation Source [48] currently under construction in Lund, Sweden. The most inefficient way to utilize a pulsed instrument is to measure a single wavelength at a time, e.g. when no ToF detector is available [38,49]. The great advantage of pulsed sources for imaging are, however, the efficient use of neutrons in ToF mode which enables high wavelength resolution and the quasi simultaneous measurement of extended spectra, which facilitates in-situ studies not achievable at continuous sources [20].

2.4. Experimental approaches

While this article focuses on imaging measurements in transmission, it has to be noted that several even early attempts of imaging crystalline features were based on detector geometries at distinct angles to the incident beam. Topography, where the detector is positioned in a Bragg reflection of a single crystal or large crystal grain in the vicinity of the sample was pioneered in Japan for both nuclear and magnetic scattering enabling the investigation of crystal defects and magnetic domains [52,53]. The technique was mainly applied in the 1970ties and 80ties in various studies of crystal growth striations, single crystal dislocations and ferro- and antiferromagnetic domains as comprehensively summarized by Schlenker and Baruchel [54,55]. The image contrast of lengthy exposures (10s of hours) in the weak monochromatic diffracted beam, mostly on neutron sensitive film material at that time, was based on nuclear and magnetic structure factor as well as orientation variations, and on the extinction effects dependent on crystal quality. In order to overcome the limitation of 2D images, section topography [56], a slit scanning technique, and even topo-tomography [22], both like topography in general adapted from X-ray equivalents, were attempted but faced severe exposure time limitations hindering routine applications. In general, although weak diffraction and corresponding variations are easier detected in such geometry than in transmission, the weak signal paired with the aim of high spatial resolution poses severe limitations to imaging approaches with neutrons in diffraction geometry.

A coarse spatial resolution (~3 mm) tomographic approach based on TOF diffraction detectors at a pulsed source was proposed in [57]. The technique is based on a formula used to correct for off-centre sample displacement in diffraction experiments. The method was demonstrated

by mapping the phase composition in an extended sample by a rotational scan in the neutron beam. Nevertheless, yet another tomographic approach with imaging detectors in diffraction geometry was reported recently as neutron diffraction contrast tomography [50,51]. This method aims at the reconstruction of individual crystal grains in a poly-crystalline sample, again in analogy to equivalent X-ray methods. In contrast to topography of single crystals, here a compromise has to be found between a short sample to detector distance for high spatial resolution and a long sample to detector distance to avoid diffracted beam overlaps from different grains and reflections. The relaxed spatial resolution and the use of a broad wavelength spectrum in a quasi-Laue approach enable reasonable exposure times on the one hand, but limit the number and size range of resolvable grains. While the neutron technique is certainly suited to investigate more representative sample volumes, resolutions of ~1 mm and limitations regarding mosaicity and the number of grains that can be reconstructed (proven: 12; speculated for ideal conditions: >100) still constitute major drawbacks for practical applications. In addition, it has meanwhile been proven that grain reconstructions with better spatial resolution and of a significantly larger number of grains are possible when taking advantage of a more efficient ToF approach in transmission, which can additionally be combined with complementary simultaneous diffraction measurements straightforwardly [58,59] and which has been named ToF 3D Neutron Diffraction.

2.5. Terminology

Unfortunately, here it has to be pointed out that terminology in this quickly developing field is still a source of confusion. Terms like energy/wavelength resolved, energy/wavelength selective, Bragg edge imaging and Bragg Edge Transmission (BET) are used equally to describe any transmission imaging method taking advantage of contrast mechanisms related to Bragg scattering. Therefore, the following terminology is proposed and used. Because in elastic scattering, and meanwhile also largely in imaging, neutrons are characterized and described with their wavelengths, we choose and propose the predominant use of **wavelength** instead of energy. **Wavelength resolved** measurements are all measurements in which the wavelength of the detected neutron is well defined within the limits of resolution. **Wavelength selective** can serve as a term for monochromatic measurements and for series of discrete monochromatic measurements. **Wavelength dispersive** measurements are wavelength resolved measurements that continuously cover a certain wavelength bandwidth. **Bragg edge imaging** describes spatially resolved wavelength resolved transmission measurements, which take advantage of the elastic coherent scattering signature of a polycrystalline sample in the attenuation spectrum, i.e. the wavelength dependent cross section. While this is clearly an attenuation based approach, due to the nature of the specific exploited contrast originating in diffraction, the term diffraction contrast for this kind of wavelength dependent attenuation is certainly eligible. It is therefore that contrary to the choice in the original reports, the term **diffraction contrast imaging** certainly better describes the transmission method of what is currently called 3D neutron diffraction and vice versa. For imaging methods working in diffraction instead of transmission geometry we propose the term **diffractive imaging** with potential sub-categories for topology and others. The following section will provide an overview of the manifold ways to exploit diffraction based contrast mechanism in high resolution transmission imaging.

3. Diffraction contrast and Bragg edge imaging

As described above, diffraction contrast occurs in the transmission image due to Bragg scattering from atomic lattice planes according to Bragg's law (Eq. (3)). The term diffraction contrast generally refers to intensity difference that is obtained in the transmission image due to 'missing' neutrons that are Bragg scattered away from the incident beam direction. As such, the term can be used independently of the sample structure, i.e. single crystal or polycrystalline materials. The term Bragg edge imaging implies that information is obtained from actual visible Bragg edges, which is only the case for polycrystalline samples (generally randomly orientated grains, but see 3.3, for a detailed discussion on texture).

While simple diffraction contrast can be visible in a single image – generally recorded at a single wavelength (or also at a relaxed resolution over a larger range) – Bragg edge imaging requires a stack of images, where each image is recorded at a different wavelength over a certain range, i.e. in a wavelength dispersive approach. This experimental procedure provides measurements of the wavelength dependent total cross section and for polycrystalline materials, the analysis of therein observable Bragg edge patterns can be used in particular to provide information about the crystallographic nature of the sample which will be discussed in detail in the following sections.

For single (or oligo-) crystal samples, dips in the transmitted intensity can be observed for wavelengths where Bragg's law is being fulfilled for the given crystal orientation(s) (Fig. 1(c)) that can be used to determine the orientation and mosaicity of the crystals(s) [12,60].

A perfect powder (or isotropic polycrystalline) sample of a suitable material, i.e. with sufficiently large elastic coherent cross section, will produce distinct Bragg edges in the transmission spectrum that can be used to extract information (integrated along the beam path) about the crystallographic parameters, such as phase and strain. For samples possessing a preferred crystallographic orientation (texture), the measured cross section deviates significantly from that of an isotropic sample (compare Fig. 1) making phase and strain measurements more challenging. Once again, however, the strength of diffraction contrast lies in the potential to reveal and visualize these texture changes and potential inhomogeneities. Typical applications will be discussed in the following sections.

3.1. Stress and strain

The evaluation of applied and residual stress (and strain; directly related to stress by the modulus of elasticity) is of fundamental interest for the characterization of engineering components and materials. We should reiterate that stress (and strain) is a complex tensor field that cannot be evaluated at only one point, but over a finite volume. Moreover in a polycrystalline material one should discern between continuum long-range (often termed Type I) stresses, grain-scale stresses (Type II) and sub-grain-scale stresses (Type III) [61]. There are various destructive measurement techniques for the assessment of residual stress [61–64], but when a sample cannot be destroyed and/or when applied stresses should be measured, a non-destructive measurement technique is needed. Most commonly used are diffraction methods, using either X-rays or neutrons [65,66], where neutrons have the particular strength to enable the assessment of bulk samples due to better transmission characteristics in particular for many engineering materials. These diffraction techniques measure the interplanar lattice spacing d_{hkl} (see Eq. (3)), allowing to determine the elastic strain

$$\varepsilon = \frac{\Delta d_{hkl}}{d_{hkl}} = \frac{d_{hkl} - d0_{hkl}}{d_{hkl}}. \quad (8)$$

Generally, good knowledge of the reference lattice parameter $d0_{hkl}$ is required (usually obtained by measurements of unstrained reference samples). Stress values are obtained from strain values by choosing a suitable value of the material elastic constants [64,67]. In a diffraction experiment, the measurement location ('gauge volume') can be selected in three dimensions by defining the incident and diffracted neutron beam using slits and/or radial collimators (Fig. 2A(b)). It is usually very time consuming to produce spatially resolved strain maps of large samples using neutron diffraction, as it requires scanning, measuring one "point" after the other of sometimes significant volumes. The possibility to derive two-dimensional strain maps from Bragg edge imaging

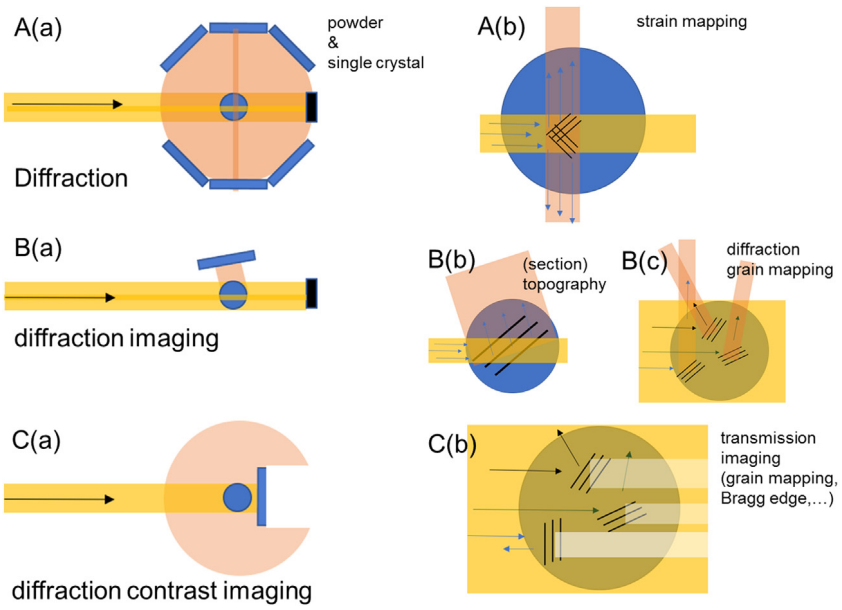

Fig. 2. Schematic of experimental neutron diffraction based approaches. (A(a)) illustrates the typical diffraction geometry, where the smaller and orthogonal scattering geometry indicates the strain scanning geometry enlarged in (A(b)) where the gauge volume is chosen by collimation of the initial and diffracted beam and the 90° geometry in both directions enables to measure two orthogonal strain directions simultaneously for correspondingly oriented crystal lattice planes in powder crystals; (B(a)) illustrates the schematic of imaging in the diffracted beam with (B(b) representing topography of single crystals and (B(c)) an approach taken in Refs. [50,51] for grain reconstruction in tomographic scans; (C(a)) outlines the transmission imaging geometry, where the field of scattered neutrons is still schematically shown, while (C(b)) illustrates the diffraction contrast in transmission and how contrast is caused by neutrons diffracted at different crystal lattice planes and orientations; a Bragg edge would be reached for a powder sample for the lowest shown scattering geometry, which underlines that strain is measured along the incident beam direction in Bragg-edge imaging; the figure furthermore exemplifies that for large enough grains, the contrast on the detector can be used to resolve the individual grains.

experiments, and the envisaged potential to expand the approach to strain tomography, has hence been an important motivating factor to develop the method originally. Additionally, since most neutron sources operate dedicated neutron strain scanners (engineering diffractometers), it appears coherent that a lot of the pioneering work related to Bragg edge imaging was performed at these instruments (see paragraph above). Fig. 2 illustrates the geometries and probed strain directions for typical diffraction setups (Fig. 2(A)) and Bragg edge transmission (compare [68]) (Fig. 2(C)).

Owing to the geometry, the two main features of strain measurements by Bragg edge transmission are that the information is averaged through the sample thickness and that the probed strain direction is always along the incident beam direction. While grains in several orientations contribute to the diffraction contrast in the transmission image, the position of the Bragg edge for a particular hkl is determined by $\lambda = 2d_{hkl}$ and hence for grains where $2\theta = 180°$. Because for this orientation the wavelength provides a direct measure for the lattice plane distance this is a very sensitive measure for lattice strain in this particular direction.

However, due to averaging over the sample thickness, it remains a challenging task to investigate complex strain fields (where the principal strain direction varies along the beam path) and components where the strain magnitude varies through the sample thickness. Because of the tensorial properties of strain, a precise determination using tomography is not straight forward. It was mathematically shown [68] that reconstruction of strain is not possible in the general sense. However, for specific cases, when certain assumptions and/or boundary conditions, such as symmetry [69–73] weighting of strain components [74] or in-situ loading [75] can be made, the tomographic reconstruction of strain components is possible.

The applicability of strain measurements by Bragg edge radiography depends on the scientific question to be answered. Fig. 3, where strain variations around a cold expanded hole in a 12 mm thick steel plate were determined, showcases an example where the through-thickness average of the out-of-plane residual elastic strain component provides valuable information [25,26]. It was shown, in particular motivated to demonstrated the accuracy of the method, that quantification of specific strain components is possible when, a-priori knowledge and/or simplifying assumptions can be applied (see Fig. 4). This applies in particular for plane stress conditions (that can arise in many practical structural engineering situations, particularly for thin samples or for compact-tension specimens used in fracture studies). For uni-axial loading in tension [44,76,77] it was shown that the derived strain component via the lattice parameter agrees with the macroscopic strain, by multiple edge refinement using time-of-flight [27] and also using a double crystal monochromator [44]. This could be used to study the elastic anisotropy in materials under tensile loading allowing the observation of local inhomogeneities during deformation, ideally in combined transmission–diffraction experiments [78].

One example provided in Ref. [41] examined projected strain measurements in the transmission direction for a standard residual stress (VAMAS “ring and plug”) sample. Utilizing a corresponding custom-made sample module in McStas, a well-established ray-tracing program for neutrons, and assigning appropriate strain values for this particular sample, it was possible to predict the ‘measured strain values’ at neutron instruments. Even though the simulation and experimental results agree well, this experiment also showcases the major shortcoming of the Bragg edge method: While in traditional (neutron) diffraction, the strain components can be measured according to their principal directions in an adaptable gauge volume, the transmission method records the projected strain, which is an average through the sample thickness. From an application point of view, quantitative values and interpretation can only be derived if the strain profile is either constant over the thickness or known, as is the case for the ring and plug sample. Correspondingly also Finite Element Modelling can aid the interpretation of results [79].

On the other hand, the key strength of imaging is the visualization of spatial differences across the FoV that can provide valuable insight. As such, the results for visualizing the residual elastic strain in bent bars [25,80–82], around cold expanded holes [25] and compact-tension specimen [80] demonstrate the potential and strengths of the technique to relevant applications. More examples are presented in Section 4 [81–83].

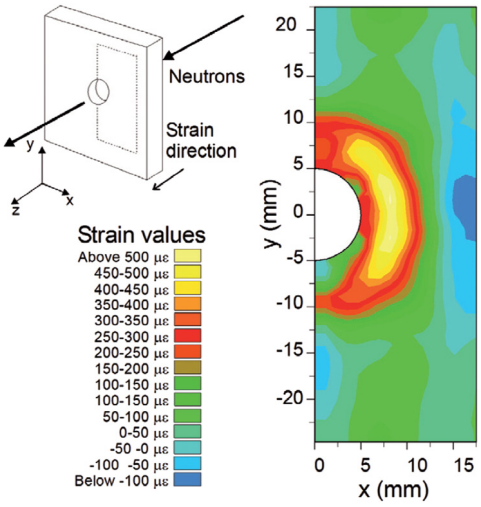

Fig. 3. Demonstration of ToF transmission measurement at ISIS showing the residual elastic strain around a cold-expanded hole in a 12 mm thick steel plate. The measured strains correspond to the through thickness average of the out-of-plane strains. The pixelated detector used in this work consists of a 10×10 array of 2×2 mm^2.
Source: Reprinted with permission of Springer from [26].

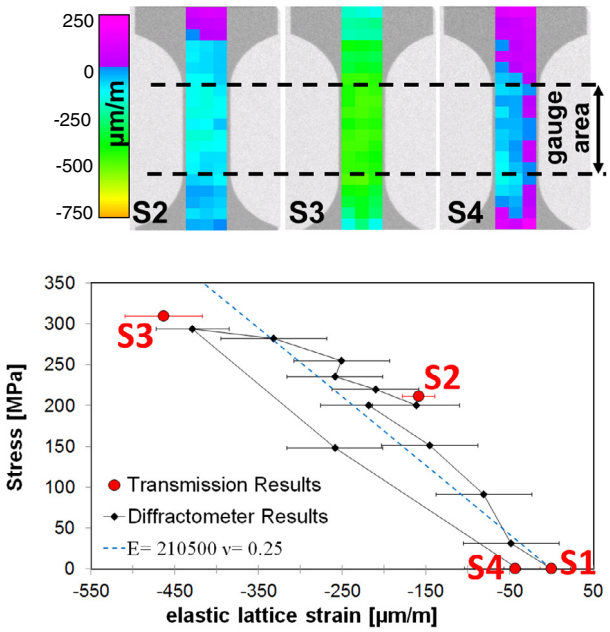

Fig. 4. Demonstration that strain can be determined even with the relaxed resolution available at a double crystal monochromator (resolution of ~3%) for a plate sample under applied tensile loading. Due to the measurement geometry, the limitation is that only the Poisson strain component can be measured in such tensile experiment.
Source: Reprinted with permission of AIP Publishing from [44].

Opportunities for strain analysis appear also for quasi single-crystal specimens such as turbine blades made of nickel superalloys. In this case, each dip observed in transmission depends on a specific sample orientation, so it is in principle possible to determine the strain with spatial resolution along several directions simultaneously. After determining the crystal orientation, the shift in wavelength position observed for each dip could enable the full determination of the strain tensor, and through the elastic constants, the associated stress tensor.

3.2. Phase analysis

While the tensorial nature of strain and small variations of the signal (shift of the Bragg edge) lead to a high level of complexity for measurements and analyses, the retrieval of crystallographic phases by neutron transmission appears more straight forward and unambiguous. At time-of-flight sources, several researchers demonstrated that crystallographic phase fractions can be determined quantitatively in transmission measurements, initially without or with very limited spatial resolution [5,6,26,30,84,85]. An early comparison of experimental results by neutron diffraction and transmission, obtained for the reversed phase transformation in austenitic stainless steel has been shown in Ref. [84].

Bragg edges associated with a certain phase (polycrystalline material) occur at several wavelengths, and imply very different attenuation coefficients for the specific phase at different distinct wavelengths. In principle, measurements taken at single wavelengths (monochromatic) can be sufficient to discriminate and quantify two (or more) phases (compare e.g. Fig. 5 and consider a wavelength of 4.1 Angstrom). In practice, however, it sometimes proves to be indispensable to record a Bragg edge spectrum that covers a broader wavelength range of one or more Bragg edges of each phase, because this enables insight if the sample e.g. exhibits or develops during a phase transition a significant texture or changing porosity, which could additionally complicate a phase determination.

While in time-of-flight measurements the wavelength coverage is less of a concern and only measurements of a certain wavelength range are efficient, it comes at the cost of much added measurement time in the case of monochromatic measurements. The common practice for measurements performed with a tunable monochromator has hence been established to initially perform a wavelength scan that covers a broad range (typically between one and several Angstroms). Based on the acquired Bragg edge patterns, one can then choose distinct wavelengths at which radiography, or even tomography, is performed with high spatial resolution. This is especially useful for in-situ studies where the monochromator approach would not allow to acquire full Bragg edge patterns fast enough, but a monochromatic time resolved measurement can suffice [86]. The advantage of using a monochromator lies in the fact that, due to the use of conventional detector systems, superior spatial resolution and large FoV's can be obtained.

On the other hand, using the time-of-flight approach, better wavelength resolution is achieved much more efficiently at pulsed sources and it is possible to probe a broad wavelength spectrum with, in principle, every neutron pulse (where additional pulses can be integrated for tailoring to the required counting statistics), hence enabling fast kinetics studies even when a wavelength dispersive measurement is required.

For samples where Bragg edges are very close to each other in the spectrum, high wavelength resolution is a requirement if these are to be resolved. This is in close analogy to a powder diffraction experiment, where sharp and narrow diffraction peaks are desired (with the width and shape of diffraction peaks depending also on beam divergence, diffraction angle and wavelength resolution).

Figs. 5 and 6 showcase the implications of using the ToF technique at spallation sources versus a monochromator at a continuous source, including the influence of utilized wavelength resolution on the Bragg edge profiles. While phase transitions can be followed in-situ using the ToF approach (Fig. 5), it can be seen that an unambiguous discrimination of mixed phases becomes challenging with the relaxed resolution of a double crystal monochromator when only a limited wavelength range can be used (Fig. 6). Results obtained for the same sample (consisting of varying amounts of Austenite and Martensite) and the same regions are compared in Fig. 6(a), where the data shown with straight lines was recorded using a double monochromator and the dotted data was recorded using the ToF technique at a short pulse neutron source. Significantly wider edges are observed in the data taken using a monochromator due to the smearing of the resolution function

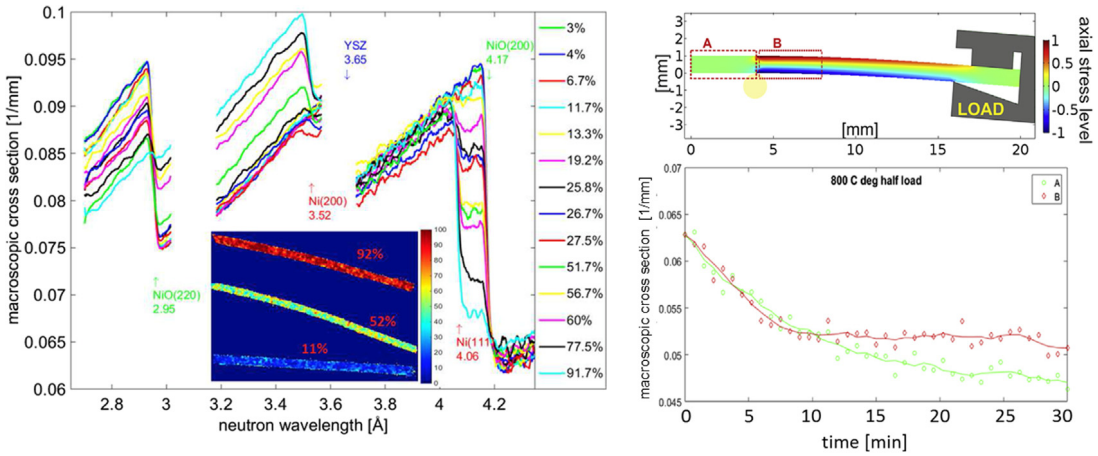

Fig. 5. In-situ phase transformation during the reduction of NiO to Ni in the NiO/Ni-YSZ anode of solid oxide cells. Left: measured macroscopic cross sections at different stages of reduction with inset of images of anodes colour coded according to Ni phase content. Reprinted with permission from [91]. Right: sample set-up for measurements in operational conditions at elevated temperatures in hydrogen atmosphere and under applied load. In the lower part the reduction behaviours over time of two different regions indicated above are compared. The effect of different strain states of these two regions can clearly be identified. (For interpretation of the references to colour in this figure legend, the reader is referred to the web version of this article.)
Source: Reprinted with permission of Electrochemical Society, Inc. from [92].

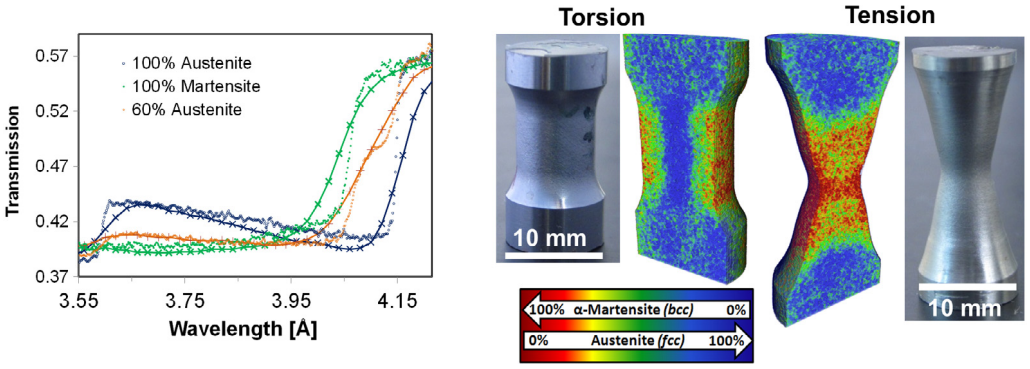

Fig. 6. Example results for samples of metastable stainless steel ('TRIP steel') that exhibit varying amounts of Austenite and Martensite after undergoing phase transformation due to plastic deformation under tension and torsion. Left: Comparison for the same sample regions (blue = 100% Austenite, green = 100% Martensite, orange = 60% Austenite) measured using a double crystal monochromator at a continuous source (straight lines, where the cross marks indicate an individual radiograph taken at that wavelength, corresponding to steps of 0.02 Å) and in time-of-flight mode at a spallation source (dots indicating where an individual image was saved) Right: Three-dimensional reconstructed phase fractions, obtained using only two wavelengths from monochromatic measurements, showing the locally varying phase transformations in samples after plastic deformation in torsion (radial varying stress distribution) and tension (where the phase distribution can be seen towards the pronounced necking region). (For interpretation of the references to colour in this figure legend, the reader is referred to the web version of this article.)
Source: Reprinted with the permission of Wiley and Sons from [87] and the International Union of Crystallography from [93].

(coarser wavelength resolution) and that for a mixed phase composition, only a single Bragg edge appears, whilst a clear shoulder is detected by ToF that separates the (110) martensitic Bragg edge and the (111) austenitic Bragg edge (compare also the results e.g. in [26]).

Nevertheless, using a double-crystal monochromator, a tomographic reconstruction of two phases in metastable stainless steel was demonstrated by recording projections at wavelengths shorter (4.1 Å) and longer (4.3 Å) than the wavelength of the corresponding (111) Bragg edge of the austenitic phase, as shown in Fig. 6(b) [87,88]. This approach, however, is yet limited to non- and mildly textured materials. For ToF data, the same approach could of course be utilized. However, wavelength resolution is at short pulse sources excessive and hence efficiency will fall short, even for significant binning in the time domain, as compared to a continuous source. However, a tomographic reconstruction of phase fractions utilizing large ranges of Bragg edge patterns has not yet been reported, even though such approach might be less prone to effects of texture. Also a full pattern refinement, such as described by Refs. [6,89,90], could be envisioned to be used to determine a phase fraction parameter for every radiographic projection that is subsequently used for a tomographic reconstruction.

While there is certainly still room for further developments in diffraction contrast imaging, applied studies of phase distributions have certainly already matured enough to represent a valuable scientific tool like underlined by a range of examples in applied materials research [91,94], cultural heritage [95], and engineering [83,96,97], which will be discussed in Section 4.

3.3. Texture analysis

The spatially resolved determination of strain and/or phase fractions from Bragg edge imaging can become very problematic when the sample under investigation exhibits a pronounced texture, as the total neutron cross section departs largely from that expected for an isotropic sample. The key strength of diffraction contrast lies here however in the ability to immediately obtain a qualitative overview of texture present and of potential local variations across the FoV, which are not

straightforwardly observed in diffraction and can hence cause wrong interpretations of results.

As discussed for the strain case, to date neutron imaging experiments alone cannot quantify a spatially varying, completely unknown ODF within a specimen, which is in general a complex function of six variables (x, y, z and three angles, e.g., the Euler angles). In this sense, diffraction contrast neutron imaging often has to be considered as a complimentary method that can reveal some aspects of this six valued function, such as local inhomogeneities that may remain undetected during conventional diffraction techniques. Diffraction techniques on the other hand can quantify the ODF through measurement of pole figures of homogeneous specimens [9]. However, this technique becomes very time consuming for the study of inhomogeneous specimens with spatially altered texture [98,99], and in the vast majority of cases requires slicing of the specimen. While it might be possible to determine pole figures and the ODF through Bragg edge imaging at least of *homogeneous* samples, i.e. without spatial variations of texture, it is not clear if that could be even as efficient than with conventional diffraction, because in most cases it could be expected to provide worse signal-to-noise ratios. On the other hand, current approaches do not yet use the full information contained in the wavelength dependent cross section and e.g. using a base of Legendre polynomials to describe the coherent elastic cross section, following the lines indicated in [100] to describe the *angular distribution function* it might be possible to efficiently retrieve ODFs efficiently and potentially also from inhomogeneous samples. However, this is a complex task and to date it has not been implemented.

On the other hand, when the ODF of a sample is known it is possible to calculate the expected transmission spectra and use the experimental transmission data to verify measurements or justify the models assumed [41,99,101,102]. In this sense, Ref. [99] suggests that Bragg edge transmission results can be used to assess the quality of texture analyses based on incomplete pole figures from diffractometers, but point out that information is averaged along the beam path which limits the application when targeting small gauge volumes.

In order to an assessment with experimental data, a model of the elastic coherent scattering cross section that actually reflects the influence of texture is needed. This can be achieved by introducing a ‘correction factor’ to Eq. (5) as was discussed in Section 2. Up to now this has been evaluated as a combination of simple models for the ODF, such as individual orientations [12], fibre textures (for example commonly found in drawn wires) [6] while additional correction factors were later included in later models [41,101,103,104] as described in Section 3.4. According to Ref. [10], for specimens with known ODFs, the transmission spectrum along different sample directions (with uniform textures) can be calculated [102] (Fig. 7).

While a full description of the ODF is not feasible from neutron transmission measurements alone, the key strength of the imaging approach is to monitor for textural inhomogeneities (Fig. 8) and observe in-situ how they change during processes. The spatial variation of texture within the bulk of metallic samples often remains inaccessible for non-destructive techniques; it is at best challenging and very time consuming. Figs. 7 and 8 illustrate the straight forward access to texture variations through diffraction contrast imaging, providing immediate qualitative assessments of inhomogeneities. The acquisition of a Bragg edge spectrum at a time-of-flight instrument is often only a matter of a few minutes and hence even allows recording several projections for improved spatial assessment (Fig. 7). It is expected that this capability can be especially useful for the optimization of new manufacturing and processing techniques, such as additive manufacturing (see applications below).

In this context it should be mentioned that the approach of using diffractive imaging or combined transmission and diffraction approaches can be seen as another step towards spatially resolved ODF studies that could be more effective than current scanning approaches [98].

3.4. Microstructure retrieval and full pattern refinement

All of the above discussed information (lattice strain, phase and texture) characterizes the microstructure of a sample and influences the measured cross sections as outlined before. However, several other parameters also impact the cross section that is measured in actual neutron transmission experiments; among them are e.g. multiple scattering and extinction effects that depend on the grain sizes present in the sample. Hence the measured spectra carry more than the before discussed information, such as information on grain sizes. Consequently, approaches for full analysis of Bragg edge transmission spectra also aim to account for all these parameters with the goal to retrieve all contained information on microstructural parameters from fitting the data by an analytical function. Such an approach is for example taken in the development of the RITS code (Rietveld Imaging of Transmission Spectra), where additional factors are introduced to Eq. (5) [89,104,105] as follows:

$$\sigma'_{coh,el}(\lambda) = \frac{\lambda^2 N}{2V_0} \sum_{hkl} |F_{hkl}|^2 d_{hkl} R_{hkl}\left(\lambda - 2d_{hkl}\right) \times P_{hkl}\left(\lambda, 2d_{hkl}\right) E_{hkl}\left(\lambda, F_{hkl}\right). \quad (9)$$

Here, the instrumental broadening, i.e. the convolution with the resolution function (which is in fact not a part of the cross section but the instrumental influence of the measurement), is described by a Jorgensen type edge profile function R_{hkl}, texture is accounted for by the March Dollase preferred orientation function P_{hkl} that is suitable for selected cases and extinction by the Sabine’s primary extinction function E_{hkl}. An example of results of derived parameters from this approach that is still under development can be seen in Fig. 9, where the degree of texture and the grain size returned by the spatially resolved analyses are depicted in corresponding images of several welded plates.

Besides the theoretical description of the total scattering cross section, the instrumental influence on the measured Bragg edges has also been addressed by Vogel using the Jorgensen type profile while Santisteban et al. [24] suggested a function based on a resolution function proposed by Kropff et al. [106], both taking into account the asymmetric intensity distribution that is characteristic to short pulse neutron sources. The ‘nxs sample’ module developed by Boin can be implemented into the established neutron ray-tracing simulation tools McStas and VITESS to predict experimentally measured cross sections at specific instruments [41,101,107]. In principle, this way even dislocation densities might become accessible to transmission imaging studies as they have significant influence on the Bragg peaks like various diffraction studies underline [108–110].

However, even without any additional quantitative analysis routines, microstructural differences can often be visualized qualitatively using diffraction contrast. Prominent examples include the visualization of differences in and around metallic welding zones [40,83,105,111–115] and in cultural heritage objects [116].

Fig. 10 shows such straight forward results for a weld and the welded plates. The rolling texture and the altered microstructure in the weld itself become obvious immediately and resemble well, although with less quantifiable detail, the partial EBSD map superimposed to the last neutron image which was taken beyond the last Bragg edge and hence without diffraction information.

In the case when single crystal samples or oligo-crystals consisting of a few grains only are investigated, characteristic dips appear in the neutron transmission spectrum as illustrated in Fig. 1(c). The dips can be used to precisely characterize the lattice parameters, the crystal orientation, the crystal mosaicity and lattice strain as demonstrated by Malamud [12] who developed a whole-pattern least-squares fitting analysis method for such spectra. Other indexing approaches for such cases are currently being used e.g. by Sato et al. [60].

However, like outlined earlier, single crystals or large grains can also be investigated in detail by diffractive imaging approaches such as topography, with the spatially resolving detector close to the crystal in a specific Bragg reflection [54,55], or by covering a wider angular range and a large number of reflections, but still with spatial resolution of the shape of the crystal [118].

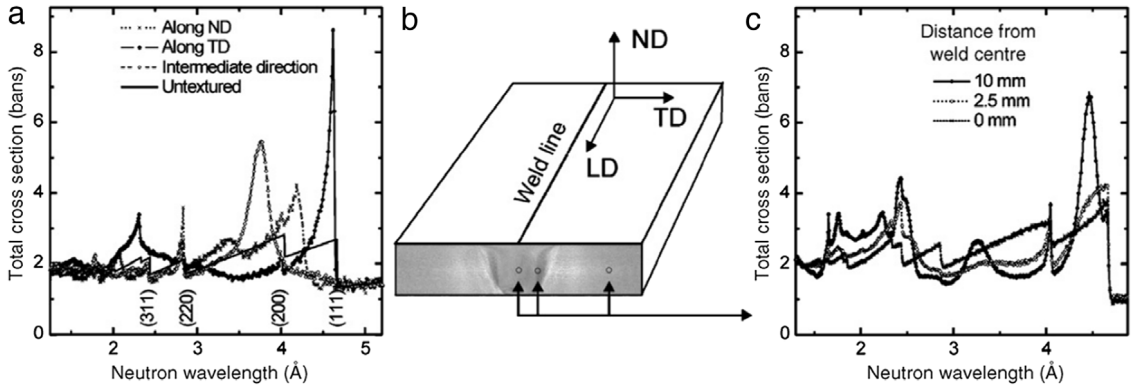

Fig. 7. ToF transmission measurements of a welded Al plate at ISIS: (a) Total cross-section along different directions compared to prediction for an untextured sample. (b) Schematic view of welded specimen. (c) Total cross-section along LD measured at the points indicated in (b). The pixelated detector used in this work consists of a 10×10 array of 2×2 mm^2. The graphs reveal large variations in edge height between different directions, e.g. the absence of the (111) edge along the normal direction (ND) means that no crystallite has directions from this family aligned to ND, while a texture of at least 6× random is revealed along the transverse direction (TD).
Source: Reprinted with permission from [10].

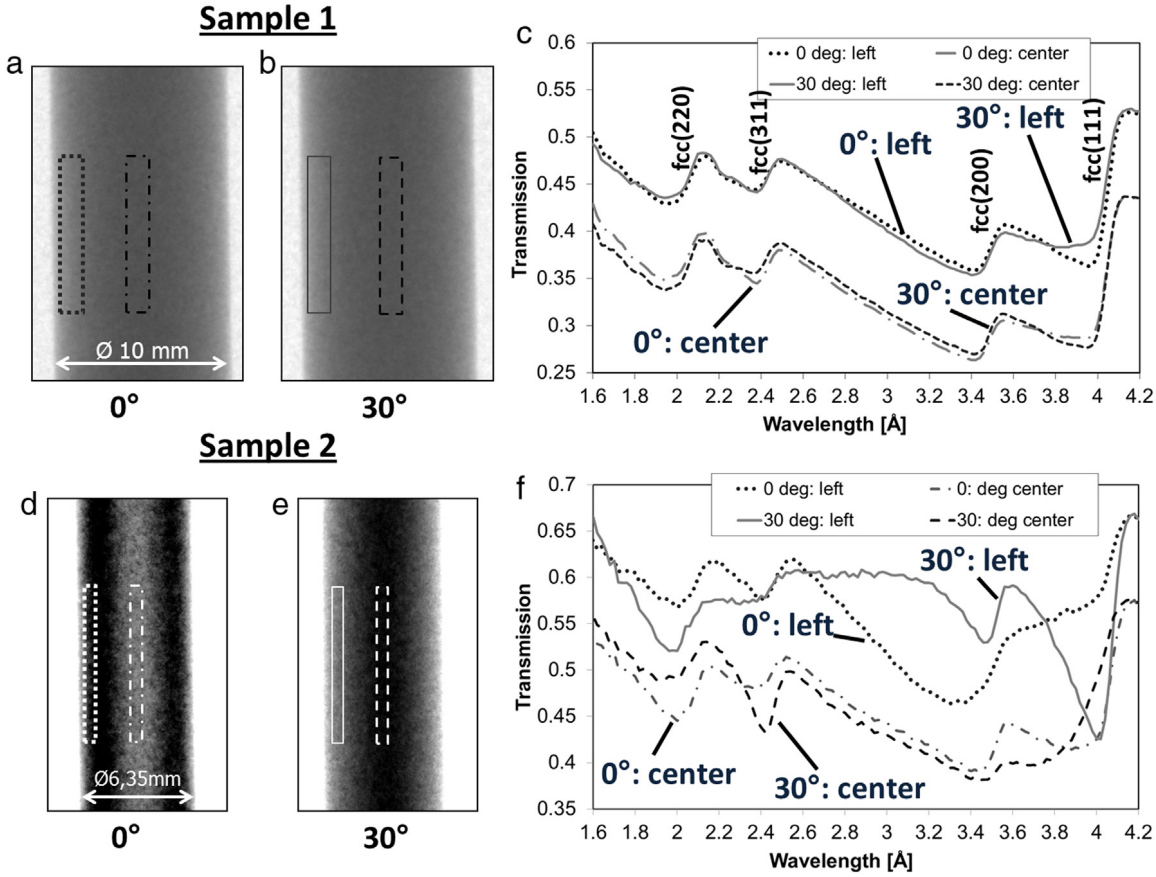

Fig. 8. Two stainless steel samples investigated by wavelength dispersive neutron radiography using a double crystal monochromator. The transmission profiles are plotted for an area in the centre of the sample and on the side. For Sample 1 (top), the Bragg edge patterns are very similar for the two sample orientations, indicating a low degree of preferred crystallite orientations. Contrary, Sample 2 (bottom) shows strongly varying Bragg edge profiles and the radiograph in (d) taken at 4 Å shows that the transmission in the centre of the sample is larger than at the side, revealing textural inhomogeneities.

3.5. Grain reconstruction

It is when the grain size in a material reaches the lower limit of the spatial resolution of a wavelength resolved transmission imaging experiment, that the Bragg edge pattern in a pixel decomposes to a pattern with distinct dips in the transmission (peaks in the cross section) spectrum (compare Fig. 1(c)). These dips are found over the full projection of an individual grain for each wavelength and orientation of a tomographic scan, where the grain fulfils the Bragg condition for a specific crystal lattice plane (*hkl*). Hence, identifying and correlating these individual projection images to the individual grains enables the

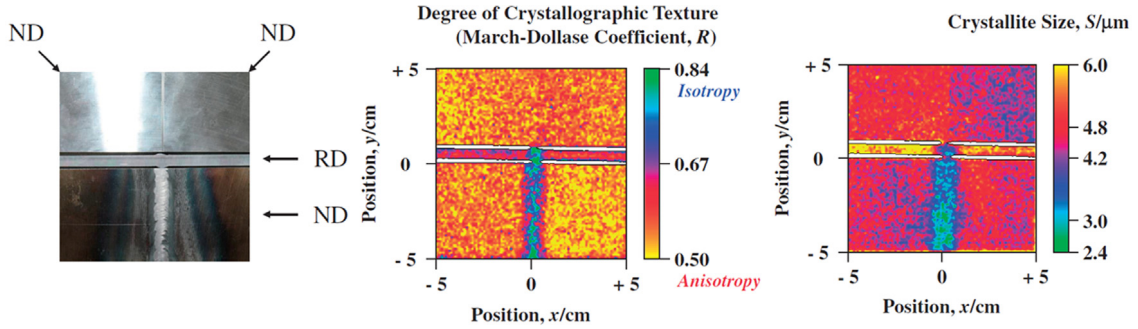

Fig. 9. Example results for rolled and welded alpha-iron plates, showing parameters that are aimed to be obtained by the RITS code through refinement of Bragg edge profiles obtained with spatial resolution.
Source: Reprinted with permission from [105].

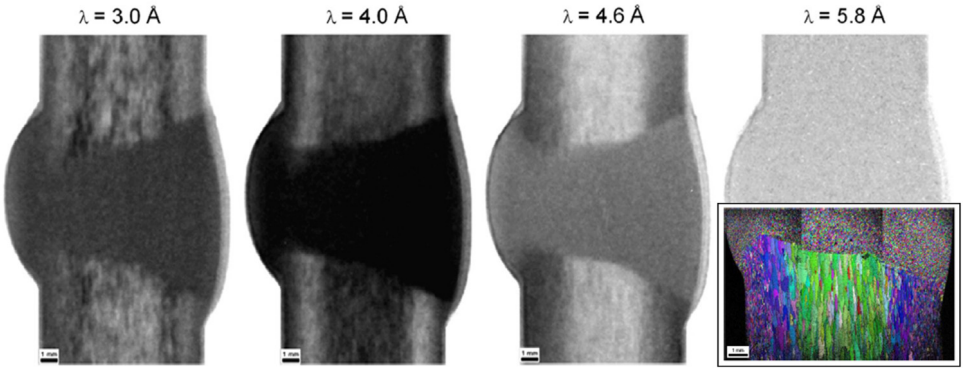

Fig. 10. Neutron-transmission images for an AL weld with 20 mm thickness where local differences in microstructure can be seen in the plate material itself as well as in the welding zone. Overlaid EBSD map from surface measurement. (Mean wavelengths are stated with 15% dispersion.)
Source: Reprinted with permission from [117].

reconstruction of the grains, and their assembly in the volume of the sample. However, in order to achieve a good sampling of each grain at many projections and to avoid severe overlaps when a large number of grains are investigated, good wavelength resolution and a wide spectral coverage are required. This transmission imaging method, which has only very recently been pioneered successfully [58,59], is hence most efficiently implemented at a pulsed source ToF instrument and appears to outperform or at least complement methods introduced earlier with detectors in diffraction geometry [50,51] as introduced in Section 2.4. Powder-like crystal regions of the sample can with this transmission method be investigated simultaneously, reconstructed separately and merged with the grain network. It has furthermore been demonstrated that a combination with large area diffraction detector coverage aides indexing and can potentially be utilized to extract further information of the individual grains [59].

4. Applications

4.1. Engineering materials research

While the type of materials that are used in engineering applications span nearly across all available material classes and rapidly expand to new and advanced materials, including e.g. nanomaterials and biomaterials [119], the vast majority of structural materials for engineering applications consist of (polycrystalline) metallic alloys. The properties of these alloys are determined by their crystallographic structure, and hence a better understanding of these properties aids the development of improved materials and processing techniques. Metallography is a well versed and manifold discipline offering a variety of established universal and specialized characterization techniques [120], while novel methods are under development continuously—especially also for three-dimensional and bulk investigations of materials. Non-destructive radiography and tomography techniques have become standard tools for the investigation of the internal structure of materials, while diffraction methods can provide more detailed information about the crystallographic properties. The benefits of combining both techniques have been realized and are routinely used in today's electron microscopes for example and they are discussed for neutrons in this review article.

Material systems that are routinely used for engineering applications are usually well characterized as they pose significant implications to structural integrity and safety (beside many others). It aided the development of the discussed novel neutron imaging techniques utilizing diffraction contrast to centre the initial applications around such widely understood material systems, e.g. in studies of phase distributions in steel systems [26,84,87] and the local strain variations in plates around structural features, including cracks and holes [26,77,79,80]. While some of these initial applications provided direct feedback for the analysis based on theoretical considerations, such as finite element and crystal plasticity models, some directly provided invaluable information on processing and manufacturing parameters, such as welding of dissimilar materials [83]. One example of the latter is presented in Fig. 11, showing the relative strain variation across a sample, consisting of a 2-mm thick steel plate autogenously laser welded to a 6-mm thick Al plate. At the same time the application demonstrated that information can be obtained from individual phases and can be combined meaningfully in one image afterwards. Moreover the study demonstrated that the distribution of elemental composition measured through resonance absorption analysis can be combined in a way similar, to what is expected to be the case for several other contrast mechanism that especially take advantage of the ToF technique [45,121]. The results from this study, that also provided insight concerning texture variations in the plate material by an analysis of Bragg edge heights and about the extent of the heat affected zone and the re-crystallization process in particular by analysis of Bragg edge widths, can be used to ensure and optimize the welding parameters.

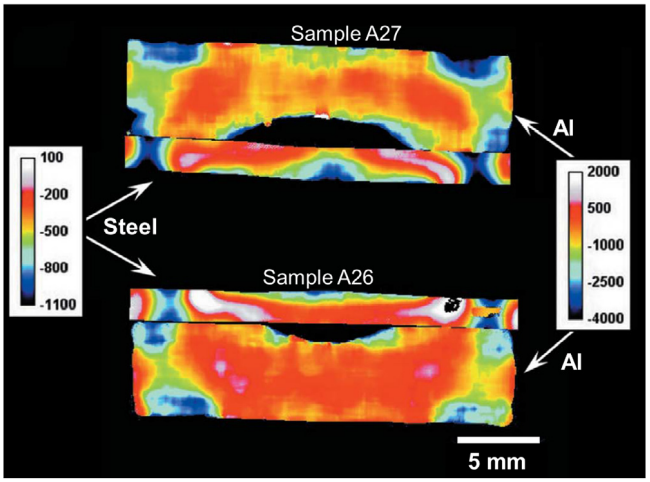

Fig. 11. Example result from the study of dissimilar weld, showing the relative strain variation across two different samples (top and bottom), where a 2-mm steel plate and a 6-mm Al plate were joined together by autogenously laser welding. The results provide information about the quality of the utilized processing parameters (different for top and bottom sample) in order to ensure that suitable thermal gradients are achieved, so that the heat conducted from the steel would only melt the aluminium in the interface region and wet the steel substrate without creating aggressive inter-diffusion of Fe and Al atoms resulting in the formation of intermetallic compounds, e.g. $FeAl_3$, $Fe2Al_5$. The fitting of the Bragg edge position does not provide reliable results for heat-affected area of the aluminium part of the weld.
Source: Reprinted with permission of the International Union of Crystallography from [83].

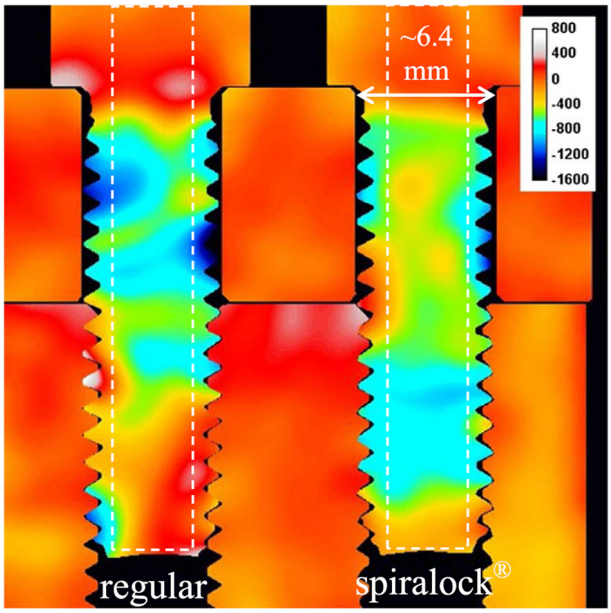

Fig. 12. Image of strain variation in an assembly consisting of two stainless (fcc) steel plates (top with through holes and bottom with female threads) and hardened (bcc) steel screws. The left connection uses a standard thread, where the stress is known to be carried non-uniformly by the thread increasing the probability of shear, and the right connection uses a Spiralock® thread, that is designed to distribute the load radially. The measured strain maps can be used for the comparison of the loads in the assemblies with respect to vibrational stability of the two thread systems.
Source: Reprinted with permission from [124].

Results of less quantitative nature are still expected to be capable of providing valuable information for the optimization of processing parameters by revealing locally varying microstructures during welding [111–113,117,122], rolling and forging processes [73,79] as well as for additive manufacturing for which an example is included in Fig. 15 [123].

Another example of phase separated strain distributions within metal structures is presented in Fig. 12, where the local strain distribution between regular and self-locking Spiralock® female threads are being compared [81]. The separate analysis of different Bragg edges and their exact positions allowed distinguishing between the ferritic steel screw and austenitic steel female thread, even though the strain is averaged through the thickness for the individual component. Such comparative studies underline how even relative (in this case strain) variations can be of significant value for the development and optimization of manufacturing processes, especially since neutrons are suitable for investigations of relevant length scales in such cases.

4.2. Applied materials research

In the development of solid oxide cells (SOC) for energy conversion either as solid oxide fuel cells (SOFC) or solid oxide electrolysis cells (SOEC) the use of Ni-YSZ cermet (yttrium stabilized zirconia) proved promising as an anode material while at the same time acting as the backbone of the cells. Often, this material is produced as NiO-YSZ and reduces to Ni-YSZ during initial operation and thus becomes electrochemically active. In addition, the reduction increases the porosity enabling efficient fuel transport through the electrode. However, it was found that upon longtime operation of SOCs these layers tend to crack and fail, which limits the lifetime of the cells. The cells are operated at elevated temperatures of around 800 °C and develop significant inner strain fields due to mismatching thermal expansion coefficients of different layers involved (anode, electrolyte, cathode). Initial mechanical testing revealed extreme creep rates in the otherwise brittle anode material during reduction, an effect dubbed accelerated creep [125]. In order to investigate and better understand the distinct behaviour of the material under stress and reduction conditions in detail an extensive study was conducted utilizing wavelength resolved transmission imaging. The material as produced and during reduction does not display a significant texture and hence the recorded Bragg edges can be analysed as to reveal the phase ratios of Ni/NiO [91] and hence the status of reduction in in-situ radiographic measurements [126] as shown in Fig. 5. Spatial resolution is required to (i) observe the spatial variation of reduction in a non-uniform strain field of the loaded samples and (ii) follow the sample spatially as it starts to deform under load during reduction [126]. It was demonstrated in various studies of dependencies on temperature, hydrogen concentration, load and redox cycling, that both ToF and monochromatic studies provided highly relevant insights. Amongst others it was clearly shown, that besides temperature and hydrogen concentration, stress also had a significant influence on the reduction kinetics, and that re-oxidation had a significant effect on developing inhomogeneous phase distributions, additional inner strains in the material and structural damage [92].

Zirconium alloys are of significant relevance in nuclear technology in particular as cladding material of fuel rods in nuclear power plants. Besides its high hardness and corrosion resistance Zirconium displays a low absorption cross section for thermal neutrons, more than an order of magnitude lower than e.g. iron. Zirconium alloys are exposed to very high levels of irradiation during the service lifetime of components in nuclear facilities. The crystallographic texture of Zr-based components is defined by the thermomechanical treatment during the manufacturing processes and has a significant influence on critical material characteristics like irradiation-growth and creep in nuclear applications. As representations in Fig. 13 exemplify, ToF imaging studies enable the spatially resolved assessment of crystallographic texture variations within such components and their dependence on production conditions like the inhomogeneous stress distributions that occur during manufacturing [102]. This initial study has underlined the potential of the method to characterize significant crystallographic

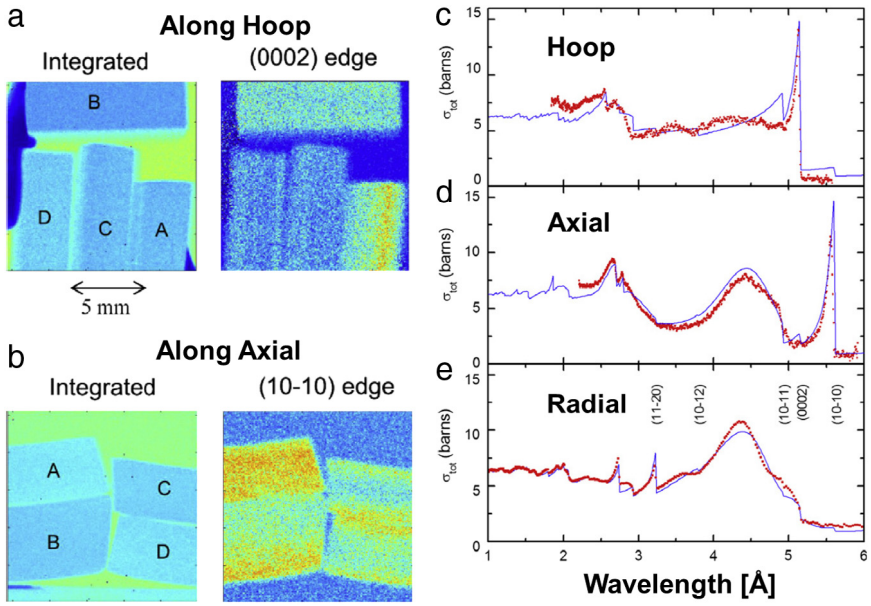

Fig. 13. (a) and (b) on the left hand side display radiographic images of pressure tube specimen in two different orientations, respectively, each for an integrated spectrum and in terms of the analysed respective Bragg edge height; the graphs on the right hand side display the measured and from pole figures calculated spectra at different orientations of sample "A". *Source:* Reprinted with permission from [102].

features of this applied material and to aid manufacturing process optimization as well as component assessment. These investigations have also an important impact on the study of hydrogen in Zr, which is a critical issue for nuclear fuel claddings in the case of corrosion and in loss-of-coolant accidents. While hydrogen uptake can be studied by conventional neutron imaging [127–129], the wavelength dispersive approach can account for influences by texture variations.

4.3. Research & development applications

The development of sufficient and long-lived energy storage devices has gained significant importance for society. Neutron science including neutron imaging is making significant contributions in this field. Examples are numerous studies in the field of Li-ion batteries, in particular utilizing neutron diffraction and conventional neutron imaging. While neutron diffraction enables observations e.g. of the status of intercalation of Li in the anode during charge and discharge [130], neutron imaging helps observing e.g. the overall distribution of Li in the battery system [131,132] depending on the state of charge. Also Li exchange between the layers has been investigated with neutron imaging [133,134]. The potential to employ wavelength resolved imaging in order to study the crystallographic effects observed in diffraction with the spatial resolution of transmission imaging was applied successfully only recently [135]. A commercial cylindrical Li-ion battery was measured by ToF imaging. While the conventional transmission image mainly revealed the redistribution of electrolyte on the macroscopic scale (Fig. 14(a)), it was also possible to observe the status of Li intercalation in the carbon anode, through local analyses of the transmission spectra (Fig. 14(b)). Although the signature of LiC_6 and LiC_{12} are very weak despite averaging the signal over areas of about 2×20 mm^2, the potential of such studies of the local behaviour in commercial systems with crystallographic resolution has clearly been demonstrated. The source at which the study has been performed is still operated significantly below the power target and instrumentation was not yet optimized. This first study utilizing diffraction contrast for spatially resolved investigations of commercial batteries hence implies a sustainable promise for future investigations in this key technology area.

Another and quickly developing and emerging field, where neutrons are applied is Metal Additive Manufacturing (AM), or 3D printing, that offers the possibility to produce complex parts without the design constraints of traditional manufacturing routes. While AM was initially seen as tool for rapid prototyping, it has now expanded for manufacturing of parts for various industries [136–138]. The fast emerging possibilities to use AM components for a wide array of applications exposes these at the same time to many different structural and mechanical requirements. The optimization of the AM processing parameters for these individual applications can be seen as key requirement and neutron imaging is expected to be capable for providing invaluable information e.g. about local variations of the microstructure. One early application example is presented in Fig. 15, where the crystallographic orientation of grains within a block of nickel base superalloy, Inconel 718, was controlled by the AM processing parameters and could clearly be retrieved through diffraction contrast imaging [123].

4.4. Cultural heritage

While non-destructive methods are the key for enabling e.g. in-situ studies, for cultural heritage artefacts non-destructive methods are very often the only option for in-depth studies of invaluable archaeological objects. The investigation of the microscopic structure of crystalline materials can give an insight on their manufacturing history [139,140] and therefore enables diffraction contrast imaging applications in an archaeological context [141–144]. Features revealed or enhanced in transmission by the wavelength resolved cross section cannot only be found in metals and alloys, but potentially in many archaeological materials that are polycrystalline like pottery, pigments, marbles, and mineralizations [145].

One example obtained by the application of the RITS code for analyses (see Section 3.5) demonstrates how Bragg edge transmission imaging is used to investigate the microstructural variations of a Japanese sword [143] from the cutting edge to the backside shedding light on the manufacturing technique. In addition, wavelength resolved imaging has helped in discriminating between and localization of different materials in artefacts as, for example, in radiographs of an ancient brooch [146], where the detection of the local Ag content is possible due to enhanced contrast due to diffraction in transmission images.

The elemental composition of alloys like bronzes ($Cu_{1-x}Sn_x$) can be determined by the lattice parameters, as in substitutional solid solutions; when bigger atoms (Sn) replace smaller atoms (Cu) the lattice

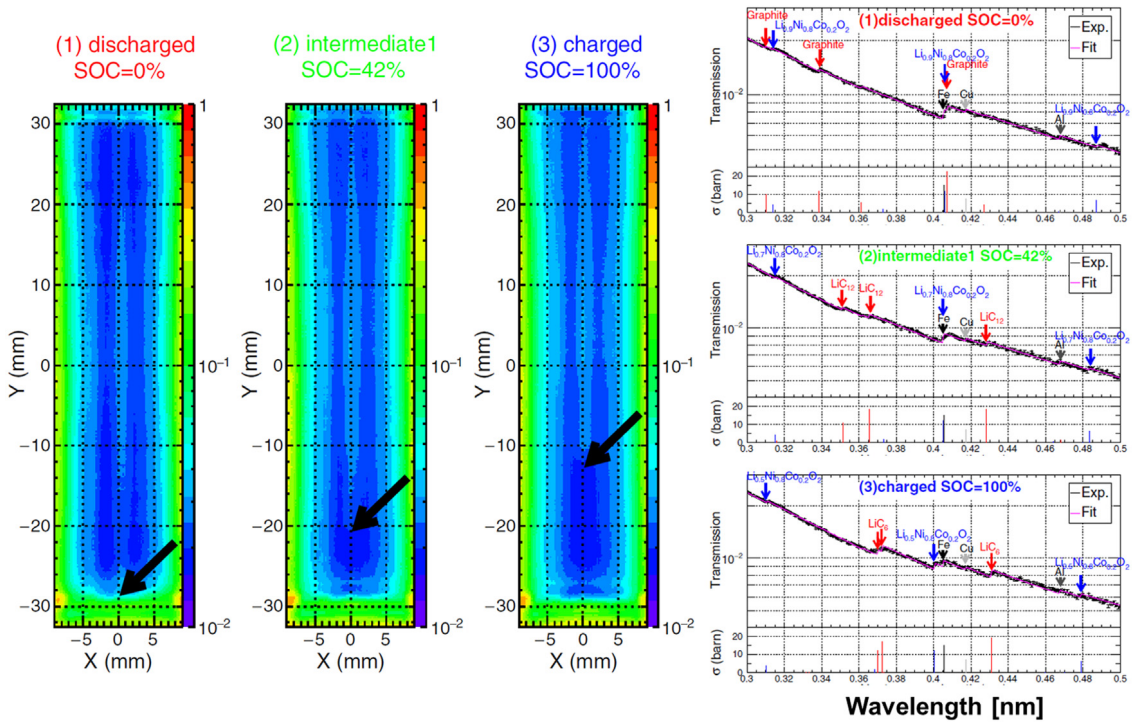

Fig. 14. Neutron transmission imaging of a commercial cylindrical battery at different states of charge. (a) Conventional transmission images displaying mainly the electrolyte distribution. (b) Corresponding transmission spectra at different regions of the battery revealing the lithiation state of the carbon anode by corresponding Bragg edges. Changes between the spectra are highlighted and the corresponding crystalline phases indicated.
Source: Reprinted with permission from [135].

parameter stretches linearly with the amount of substitute according to the Vegard's law. Although archaeological bronzes are far from being pure binary (e.g. Cu–Sn and Cu–Zn) or ternary (e.g. Cu–Sn–Zn and Cu–Sn–Pb) alloys, Bragg edge imaging is able to determine their lattice parameters with high accuracy [142], allowing for an estimate of the elemental composition of an artefact, as shown for a Shin period (1736–1796) Chinese coin [144]. Diffraction contrast transmission imaging can therefore help answering important archaeological questions related to dating and provenance as different types of bronze characterize different eras in history; moreover, it can help distinguishing raw casting from hammered and annealed bronzes [142]. A significant advantage of Bragg edge transmission imaging with respect to conventional diffraction in archaeology is the possibility of mapping the whole artefact or significant parts of them, at once, achieving a 2D image consisting of Bragg edge spectra, with sub-millimetre spatial resolution. Neutron diffraction instead is generally performed on only a few points of the artefact, with pencil beams ranging 5×5 to 40×40 mm^2, providing information with a comparatively low spatial resolution. Correct positioning of bulk and valuable historical objects in the beam is another potential issue that is easier overcome in transmission.

The ability of wavelength resolved imaging to also detect the presence of large single crystal grains which show up as low intensity spots for specific wavelengths has been applied for example on Japanese arrow heads [147] and patter welded swords [95], and revealed prolonged high temperature treatments.

Tomographies revealing the local phase variations of archaeological objects have very successfully been applied to multi-phase artefacts of historical armour and weapons in studies in particular of Japanese swords [116] and the pattern welded Viking swords [95], where composite materials were used to achieve better mechanical properties and/or particular aesthetic features. Being able to detect differences in phase compositions allows the gathering of information on manufacturing traditions, mechanical properties and even the original purpose of the artefact [95,116,144]. An example of an application to a Viking sword [95] is provided in Fig. 16, where it helped to enhance the

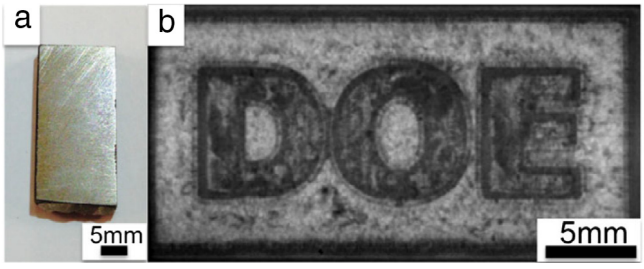

Fig. 15. The local orientation of grains in certain locations was controlled in a block made from INCONEL 718 by the electron beam melting. The region within the letters (DOE) comprises a mix of columnar and equiaxed grain growth, where the outline of the letters has a highly misoriented equiaxed grain growth and the region outside the letters exhibits preferred ⟨001⟩ columnar solidification grain growth.
Source: Reprinted with permission of Taylor & Francis Ltd, www.tandfonline.com on behalf of The Institute of Materials, Minerals and Mining from [123].

distribution of ferritic phase and remove the contribution from corrosion phases; the section shows almost pure ferritic edges rather than harder steel edges, and numerous slag impurities in the core, suggesting that pattern welded swords in the Viking age had mainly symbolic purposes.

5. Outlook

The discovery of the huge potential for applications of diffraction contrast measurements with high spatial image resolution led to significant changes in the instrumentation of in particular the leading imaging facilities around the globe as well as to the introduction of novel ToF imaging instruments at the new powerful pulsed spallation sources worldwide. Within a few years after the first double crystal monochromator was installed at CONRAD at Helmholtz Zentrum Berlin (HZB) [32], similar devices for wavelength resolved applications have subsequently also been installed at the imaging instruments of the continuous neutron sources of FRM2 [115] PSI, NIST [148] etc. and

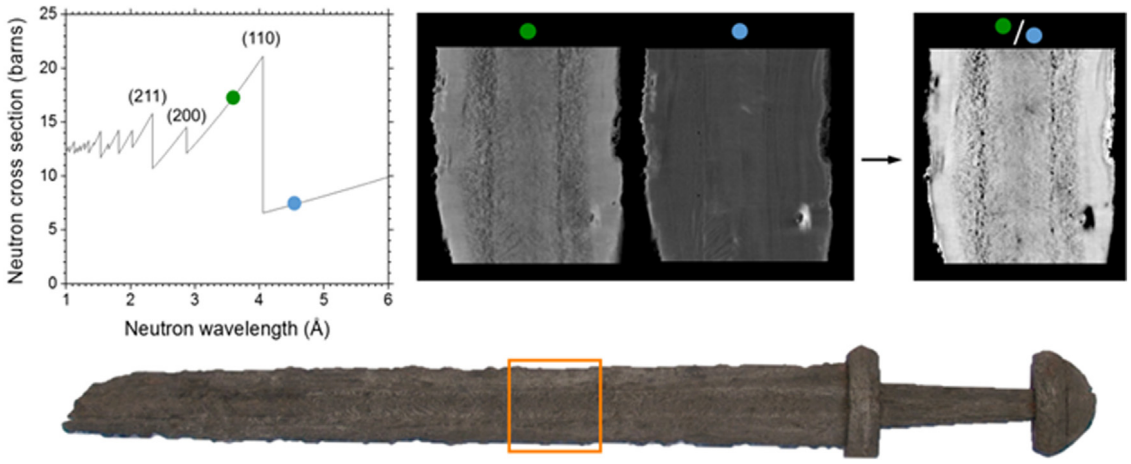

Fig. 16. Two tomographies are taken just below and after the (110) ferrite Bragg edge; the ratio between the two is able to enhance ferrite, while corrosion phases become transparent as their attenuation coefficients are equal at the two wavelengths [95].
Source: Reprinted with permission of Springer from [95].

enabled a number of novel wavelength resolved imaging methods such as e.g. polarized neutron imaging [149]. What is maybe even more important is the fact that the successful ToF applications triggered neutron imaging instrumentation at the new powerful pulsed spallation neutron sources like at the second target station (TS2) at ISIS (IMAT, UK) [150] and JPARC (RADEN. Japan) [151,152], where pioneering instruments are in the phase of commissioning. Instruments at the SNS (VENUS, US) [153] and the European Spallation Source (ODIN, Sweden) [48], the first long pulse spallation source, are under construction. The number of applications is growing and still pushing the boundaries in resolution, measurement and instrument optimization and particular in analyses and quantification. While some limitations are inherent to the transmission technique, a lot more information content can still be utilized with thorough analytic approaches and analyses tools, a number of which is under development. The new instruments at spallation sources in particular carry a promise to enable more and better in-situ studies, which, however, also imply the need of development of corresponding sample environment, optimized to the transmission geometry and playing to the strength of neutron applications [78,154]. The optimized flux conditions that are expected once the new sources reach their full power indicate the potential of further progress. Besides further improving resolutions in spatial and reciprocal space, especially an improved time resolution is expected to enable unprecedented kinetic studies.

A key technological bottleneck still concerns the detector technology for high spatial and ToF resolution, especially with view on increasing flux conditions and limitations in the field of view. The borated MCP (microchannel plate) detector technology together with the arrival of the new generation of timepix3 chips might enable to overcome the first issue and a combination of more than the current four chips could increase the FoV at least in one direction. However, also alternative developments are required and a few of them are well on the way, offering different combinations of FoV and spatial resolution [35,155–157], but also sometimes severe deficiencies e.g. in efficiency. Additionally, it shall be mentioned, that the instrument IMAT and some instruments under construction at ESS, intend to combine transmission neutron imaging with significant diffraction detector coverage. The first works in this regards at SENJU at JPARC [58] underline the potential of such approaches, which are not yet even fully predictable and are expected to open up unprecedented possibilities.

We hope that, within this review, we were able to provided a good overview over this vivid and emerging field of spatially resolved imaging studies of crystalline features, covering a wide range of applications from applied material science, engineering research, magnetism and even archaeology, while outlining some perspectives and recent developments that promise far more to come.

Acknowledgements

Numerous invaluable and interesting discussion with Sven Vogel, Winfried Kockelmann, Malgorzata Makowska, Francesco Grazzi, Soren Schmidt, Mirko Boin, Dayakar Penumadu and Nikolay Kardjilov, beside many others are very much appreciated.

References

[1] W. Bragg, W. Bragg, The reflection of X-rays by crystals, Proc. R. Soc. Lond. Ser. A 88 (1913) 428–438.
[2] W.L. Bragg, The structure of some crystals as indicated by their diffraction of X-rays, Proc. R. Soc. Lond. Ser. A 89 (1913) 248–277.
[3] R.E. Dinnebier, Powder Diffraction: Theory and Practice, Royal Society of Chemistry, 2008.
[4] V.K. Pecharsky, P.Y. Zavalij, Fundamentals of Powder Diffraction and Structural Characterization of Materials, Springer, 2009.
[5] A. Steuwer, P.J. Withers, J.R. Santisteban, L. Edwards, Using pulsed neutron transmission for crystalline phase imaging and analysis, J. Appl. Phys. 97 (2005) 074903.
[6] S. Vogel, A Rietveld-Approach for the Analysis of Neutron Time-of-Flight Transmission Data, Mathematisch-Naturwissenschaftliche Fakultät, Ph.D. thesis, Uni Kiel, Kiel, 2000, pp. 174.
[7] O. Halpern, M. Hamermesh, M. Johnson, The passage of neutrons through crystals and polycrystals, Phys. Rev. 59 (1941) 981.
[8] E. Fermi, W.J. Sturm, R.G. Sachs, The transmission of slow neutrons through microcrystalline materials, Phys. Rev. 71 (1947) 589–594.
[9] U.F. Kocks, C.N. Tomé, H.-R. Wenk, Texture and Anisotropy: Preferred Orientations in Polycrystals and their Effect on Materials Properties, Cambridge University Press, 2000.
[10] J.R. Santisteban, L. Edwards, V. Stelmukh, Characterization of textured materials by TOF transmission, Physica B 385–386 (Part 1) (2006) 636–638.
[11] R.J. Weiss, J.R. Clark, L. Corliss, J. Hastings, Neutron diffraction studies of cold-worked brass, J. Appl. Phys. 23 (1952) 1379–1382.
[12] F. Malamud, J.R. Santisteban, Full-pattern analysis of time-of-flight neutron transmission of mosaic crystals, J. Appl. Crystallogr. 49 (2016).
[13] L. Winsberg, D. Meneghetti, S.S. Sidhu, Total neutron cross sections of compounds with different crystalline structures, Phys. Rev. 75 (1949) 975–979.
[14] J. Cassels, The scattering of neutrons by crystals, Prog. Nucl. Phys. (1950) editor OR.
[15] R. Johnson, C. Bowman, High resolution powder diffraction by white source transmission measurements, AIP Conf. Proc. 89 (89) (1982) 53–56.
[16] K. Meggers, H.G. Priesmeyer, W.J. Trela, C.D. Bowman, M. Dahms, Real time neutron transmission investigation of the austenite-bainite transformation in grey iron, Nucl. Instrum. Methods Phys. Res. B 88 (1994) 423–429.
[17] K. Meggers, H.G. Priesmeyer, W.J. Trela, M. Dahms, Investigation of the austenite-bainite transformation in gray iron using real time neutron transmission, Mater. Sci. Eng. A 188 (1994) 301–304.
[18] D.Q. Wang, Strain Measurement Using Neutron Diffraction, The Open University, 1996.
[19] H.G. Priesmeyer, M. Stalder, S. Vogel, K. Meggers, R. Bless, W. Trela, Bragg-Edge transmission as an additional tool for strain measurements, Textures Microstruct. 33 (1999) 173–185.

[20] M.E. Fitzpatrick, A. Lodini, Analysis of Residual Stress by Diffraction Using Neutron and Synchrotron Radiation, CRC Press, 2003.
[21] J.R. Santisteban, L. Edwards, H.G. Priesmeyer, S. Vogel, Comparison of Bragg-Edge neutron-transmission spectroscopy at ISIS and LANSCE, Appl. Phys. A Mater. Sci. Process. 74 (2002) s1616–s1618.
[22] N. Kardjilov, Further developments and applications of radiography and tomography with thermal and cold neutrons, Universität München, Ph.D. thesis, 2003.
[23] N. Kardjilov, S. Baechler, M. Bastürk, M. Dierick, J. Jolie, E. Lehmann, T. Materna, B. Schillinger, P. Vontobel, New features in cold neutron radiography and tomography Part II: applied energy-selective neutron radiography and tomography, Nucl. Instrum. Methods Phys. Res., Sect. A 501 (2003) 536–546.
[24] J.R. Santisteban, L. Edwards, A. Steuwer, P.J. Withers, Time-of-flight neutron transmission diffraction, J. Appl. Crystallogr. 34 (2001) 289–297.
[25] J.R. Santisteban, L. Edwards, M.E. Fitzpatrick, A. Steuwer, P.J. Withers, M.R. Daymond, M.W. Johnson, N. Rhodes, E.M. Schooneveld, Strain imaging by Bragg edge neutron transmission, Nucl. Instrum. Methods Phys. Res., Sect. A 481 (2002) 765–768.
[26] J.R. Santisteban, L. Edwards, M.E. Fizpatrick, A. Steuwer, P.J. Withers, Engineering applications of Bragg-edge neutron transmission, Appl. Phys. A 74 (2002) s1433–s1436.
[27] A. Steuwer, P.J. Withers, J.R. Santisteban, L. Edwards, G. Bruno, M.E. Fitzpatrick, M.R. Daymond, M.W. Johnson, D. Wang, Bragg edge determination for accurate lattice parameter and elastic strain measurement, Phys. Status Solidi (a) 185 (2001) 221–230.
[28] A. Steuwer, J.R. Santisteban, P.J. Withers, L. Edwards, M.E. Fitzpatrick, In situ determination of stresses from time-of-flight neutron transmission spectra, J. Appl. Crystallogr. 36 (2003) 1159–1168.
[29] N. Kardjilov, B. Schillinger, E. Steichele, Energy-selective neutron radiography and tomography at FRM, Appl. Radiat. Isot. 61 (2004) 455–460.
[30] A. Steuwer, J.R. Santisteban, P.J. Withers, L. Edwards, Pattern decomposition and quantitative-phase analysis in pulsed neutron transmission, Physica B 350 (2004) 159–161.
[31] J.R. Santisteban, A. Steuwer, L. Edwards, P.J. Withers, M.E. Fitzpatrick, Mapping of unstressed lattice parameters using pulsed neutron transmission diffraction, J. Appl. Crystallogr. 35 (2002) 497–504.
[32] W. Treimer, M. Strobl, N. Kardjilov, A. Hilger, I. Manke, Wavelength tunable device for neutron radiography and tomography, Appl. Phys. Lett. 89 (2006) 203504.
[33] A.S. Tremsin, W. Bruce Feller, R. Gregory Downing, Efficiency optimization of microchannel plate (MCP) neutron imaging detectors. I. Square Channels with 10B Doping., Nucl. Instrum. Methods Phys. Res., Sect. A 539 (2005) 278–311.
[34] A.S. Tremsin, J.V. Vallerga, J.B. McPhate, O.H.W. Siegmund, W.B. Feller, L. Crow, R.G. Cooper, On the possibility to image thermal and cold neutron with sub-15 μm spatial resolution, Nucl. Instrum. Methods Phys. Res., Sect. A 592 (2008) 374–384.
[35] Y. Kiyanagi, T. Kamiyama, K. Kino, H. Sato, S. Sato, S. Uno, Pulsed neutron imaging using 2-dimensional position sensitive detectors, J. Instrum. 9 (2014) C07012.
[36] M. Strobl, I. Manke, N. Kardjilov, A. Hilger, M. Dawson, J. Banhart, Advances in neutron radiography and tomography, J. Phys. D: Appl. Phys. 42 (2009) 243001.
[37] S.H. Williams, A. Hilger, N. Kardjilov, I. Manke, M. Strobl, P.A. Douissard, T. Martin, H. Riesemeier, J. Banhart, Detection system for microimaging with neutrons, J. Instrum. 7 (2012) P02014.
[38] M. Strobl, A. Hilger, M. Boin, N. Kardjilov, R. Wimpory, D. Clemens, M. Mühlbauer, B. Schillinger, T. Wilpert, C. Schulz, K. Rolfs, C.M. Davies, N. O'Dowd, P. Tiernan, I. Manke, Time-of-flight neutron imaging at a continuous source: Proof of principle using a scintillator CCD imaging detector, Nucl. Instrum. Methods Phys. Res., Sect. A 651 (2011) 149–155.
[39] M. Strobl, R. Woracek, N. Kardjilov, A. Hilger, R. Wimpory, A. Tremsin, T. Wilpert, C. Schulz, I. Manke, D. Penumadu, Time-of-flight neutron imaging for spatially resolved strain investigations based on Bragg edge transmission at a reactor source, Nucl. Instrum. Methods Phys. Res., Sect. A 680 (2012) 27–34.
[40] E.H. Lehmann, G. Frei, P. Vontobel, L. Josic, N. Kardjilov, A. Hilger, W. Kockelmann, A. Steuwer, The energy-selective option in neutron imaging, Nucl. Instrum. Methods Phys. Res., Sect. A 603 (2009) 429–438.
[41] M. Boin, Developments Towards the Tomographic Imaging of Local Crystallographic Structures, Open University. Ph.D. thesis, 2010.
[42] S. Peetermans, F. Grazzi, F. Salvemini, E. Lehmann, Spectral characterization of a velocity selector type monochromator for energy-selective neutron imaging, Phys. Procedia 43 (2013) 121–127.
[43] S.L.X. Peetermans, Energy-Selective Neutron Imaging for Materials Science, EPFL, 2015.
[44] R. Woracek, D. Penumadu, N. Kardjilov, A. Hilger, M. Strobl, R.C. Wimpory, I. Manke, J. Banhart, Neutron Bragg-edge-imaging for strain mapping under in situ tensile loading, J. Appl. Phys. 109 (2011) 093506.
[45] M. Strobl, Future prospects of imaging at spallation neutron sources, Nucl. Instrum. Methods Phys. Res., Sect. A 604 (2009) 646–652.
[46] M. Strobl, M. Bulat, K. Habicht, The wavelength frame multiplication chopper system for the ESS test beamline at the BER II reactor—A concept study of a fundamental ESS instrument principle, Nucl. Instrum. Methods Phys. Res., Sect. A 705 (2013) 74–84.
[47] R. Woracek, T. Hofmann, M. Bulat, M. Sales, K. Habicht, K. Andersen, M. Strobl, The testbeamline of the European Spallation Source–instrumentation development and wavelength frame multiplication, Nucl. Instrum. Methods Phys. Res., Sect. A (2016).
[48] M. Strobl, The scope of the imaging instrument project ODIN at ESS, Phys. Procedia 69 (2015) 18–26.
[49] W. Kockelmann, G. Frei, E.H. Lehmann, P. Vontobel, J.R. Santisteban, Energy-selective neutron transmission imaging at a pulsed source, Nucl. Instrum. Methods Phys. Res., Sect. A 578 (2007) 421–434.
[50] S. Peetermans, A. King, W. Ludwig, P. Reischig, E. Lehmann, Cold neutron diffraction contrast tomography of polycrystalline material, Analyst 139 (2014) 5766–5772.
[51] D. Penumadu, R. Woracek, Accomplishments and future needs for enery selective neutron imaging considering diffraction contrast, Neuwave 5, Lund, Swedem, 2013.
[52] K. Doi, N. Minakawa, H. Motohashi, N. Masaki, A trial of neutron diffraction topography, J. Appl. Crystallogr. 4 (1971) 528–530.
[53] M. Ando, S. Hosoya, Q-switch and polarization domains in antiferromagnetic Chromium observed with neutron-diffraction topography, Phys. Rev. Lett. 29 (1972) 281.
[54] M. Schlenker, J. Baruchel, Neutron topography: A review, Physica B + C 137 (1986) 309–319.
[55] J. Baruchel, Neutron topography, Neutron News 3 (1992) 20–25.
[56] H. Tomimitsu, A neutron diffraction topographic observation of strain field in a hot-pressed germanium crystal, J. Appl. Crystallogr. 7 (1974) 59–64.
[57] M.J. Gutmann, W. Kockelmann, L.C. Chapon, P.G. Radaelli, Phase imaging using time-of-flight neutron diffraction, J. Appl. Crystallogr. 39 (2006) 82–89.
[58] A. Cereser, Time-of-flight 3D Neutron Diffraction for Multigrain Crystallography, DTU Department of Physics, Ph.D. thesis, Technical University of Denmark, 2016.
[59] Alberto Cereser, Markus Strobl, Stephen Hall, Axel Steuwer, Ryoji Kiyanagi, Anton Tremsin, Erik Bergbäck Knudsen, Takenao Shinohara, Peter Willendrup, Alice Bastos da Silva Fanta, Srinivasan Iyengar, Peter Mahler Larsen, Takayasu Hanashima, Taketo Moyoshi, Peter M. Kadletz, Philip Krooß, Thomas Niendorf, Morten Sales, Wolfgang W. Schmahl, S. Schmidt, Sci. Rep. (2017) in preparation.
[60] H. Sato, Grain orientation imaging by pulsed neutron transmission measurements, Neuwave8, Abingdon, Oxfordshire, United Kingdom, 2016.
[61] P.J. Withers, M. Turski, L. Edwards, P.J. Bouchard, D.J. Buttle, Recent advances in residual stress measurement, Int. J. Press. Vessels Pip. 85 (2008) 118–127.
[62] R. Leggatt, D. Smith, S. Smith, F. Faure, Development and experimental validation of the deep hole method for residual stress measurement, J. Strain Anal. Eng. Des. 31 (1996) 177–186.
[63] G.S. Schajer, Practical Residual Stress Measurement Methods, John Wiley & Sons, 2013.
[64] P.J. Withers, H.K.D.H. Bhadeshia, Residual stress. Part 1–Measurement techniques., Mater. Sci. Technol. 17 (2001) 355–365.
[65] M.T. Hutchings, P.J. Withers, T.M. Holden, T. Lorentzen, Introduction to the Characterization of Residual Stress By Neutron Diffraction, CRC Press, 2005.
[66] A.D. Krawitz, Neutron strain measurement, Mater. Sci. Technol. 27 (2011) 589–603.
[67] A. Krawitz, R. Winholtz, C. Weisbrook, Relation of elastic strain distributions determined by diffraction to corresponding stress distributions, Mater. Sci. Eng. A 206 (1996) 176–182.
[68] W.R. Lionheart, P.J. Withers, Diffraction tomography of strain, Inverse Problems 31 (2015) 045005.
[69] B. Abbey, S.Y. Zhang, W.J.J. Vorster, A.M. Korsunsky, Feasibility study of neutron strain tomography, Procedia Eng. 1 (2009) 185–188.
[70] B. Abbey, S.Y. Zhang, W. Vorster, A.M. Korsunsky, Reconstruction of axisymmetric strain distributions via neutron strain tomography, Nucl. Instrum. Methods Phys. Res. B 270 (2012) 28–35.
[71] B. Abbey, S.Y. Zhang, M. Xie, X. Song, A.M. Korsunsky, Neutron strain tomography using Bragg-edge transmission, Int. J. Mater. Res. 103 (2012) 234–241.
[72] H.J. Kirkwood, B. Abbey, H.M. Quiney, S.Y. Zhang, A.S. Tremsin, A. Korsunsky, Bragg edge neutron strain tomography, 2013.
[73] W. Li, S.Y. Zhang, S. Kabra, A. Tremsin, B. Abbey, H. Kirkwood, D. Terret, S. Ndoye, E.T. McDevitt, Characterisation of residual stress due to fillet rolling on bolts made of a nickel base superalloy, in: Advanced Materials Research, Trans Tech Publ, 2014, pp. 670–675.
[74] C. Wensrich, J. Hendriks, M. Meylan, Bragg edge neutron transmission strain tomography in granular systems, Strain 52 (2016) 80–87.
[75] C. Wensrich, J. Hendriks, A. Gregg, M. Meylan, V. Luzin, A. Tremsin, Bragg-edge neutron transmission strain tomography for in situ loadings, Nucl. Instrum. Methods Phys. Res. B 383 (2016) 52–58.
[76] A. Steuwer, Strain determination and imaging by pulsed neutron transmission, Department of Materials Science and Metallurgy, Ph.D. thesis, University of Cambridge, 2002.

[77] K. Iwase, H. Sato, S. Harjo, T. Kamiyama, T. Ito, S. Takata, K. Aizawa, Y. Kiyanagi, In situ lattice strain mapping during tensile loading using the neutron transmission and diffraction methods, J. Appl. Crystallogr. 45 (2012) 113–118.
[78] R. Woracek, J. Bunn, D. Penumadu, A. Tremsin, A. Siriruk, N. Kardjilov, I. Manke, M. Boin, A. Hilger, C. Hubbard, Methodology for combined neutron diffraction and bragg edge imaging, in: MRS Proceedings, Cambridge Univ Press, 2013, pp. mrsf12–1528–vv1508–1504.
[79] R. Woracek, Energy selective neutron imaging for the characterization of polycrystalline materials, The University of Tennessee, Knoxville, Ph.D. thesis, 2015.
[80] A.S. Tremsin, J.B. McPhate, A. Steuwer, W. Kockelmann, A.M. Paradowska, J.F. Kelleher, J.V. Vallerga, O.H.W. Siegmund, W.B. Feller, High-resolution strain mapping through time-of-flight neutron transmission diffraction with a microchannel plate neutron counting detector, Strain 48 (2012) 296–305.
[81] K. Iwase, K. Sakuma, T. Kamiyama, Y. Kiyanagi, Bragg-edge transmission imaging of strain and microstructure using a pulsed neutron source, Nucl. Instrum. Methods Phys. Res., Sect. A 605 (2009) 1–4.
[82] Y. Su, K. Oikawa, S. Harjo, T. Shinohara, T. Kai, M. Harada, K. Hiroi, S. Zhang, J.D. Parker, H. Sato, Y. Shiota, Y. Kiyanagi, Y. Tomota, Time-of-flight neutron Bragg-edge transmission imaging of microstructures in bent steel plates, Mater. Sci. Eng. A 675 (2016) 19–31.
[83] A.S. Tremsin, S. Ganguly, S.M. Meco, G.R. Pardal, T. Shinohara, W.B. Feller, Investigation of dissimilar metal welds by energy-resolved neutron imaging, J. Appl. Crystallogr. 49 (2016).
[84] M.A.M. Bourke, J.G. Maldonado, D. Masters, K. Meggers, H.G. Priesmeyer, Real time measurement by Bragg edge diffraction of the reverse ($\alpha' \rightarrow \gamma$) transformation in a deformed 304 stainless steel, Mater. Sci. Eng. A 221 (1996) 1–10.
[85] J. Huang, S.C. Vogel, W.J. Poole, M. Militzer, P. Jacques, The study of low-temperature austenite decomposition in a Fe–C–Mn–Si steel using the neutron Bragg edge transmission technique, Acta Mater. 55 (2007) 2683–2693.
[86] E. Dabah, B. Pfretzschner, T. Schaupp, N. Kardjilov, I. Manke, M. Boin, R. Woracek, A. Griesche, Time-resolved Bragg-edge neutron radiography for observing martensitic phase transformation from austenitized super martensitic steel, J. Mater. Sci. (2016) 1–7.
[87] R. Woracek, D. Penumadu, N. Kardjilov, A. Hilger, M. Boin, J. Banhart, I. Manke, 3D mapping of crystallographic phase distribution using energy-selective neutron tomography, Adv. Mater. 26 (2014) 4069–4073.
[88] R. Woracek, D. Penumadu, N. Kardjilov, A. Hilger, M. Boin, J. Banhart, I. Manke, Neutron bragg edge tomography for phase mapping, Phys. Procedia 69 (2015) 227–236.
[89] H. Sato, T. Shinohara, R. Kiyanagi, K. Aizawa, M. Ooi, M. Harada, K. Oikawa, F. Maekawa, K. Iwase, T. Kamiyama, Upgrade of Bragg edge analysis techniques of the RITS code for crystalline structural information imaging, Phys. Procedia 43 (2013) 186–195.
[90] Y. Kiyanagi, H. Sato, T. Kamiyama, T. Shinohara, A new imaging method using pulsed neutron sources for visualizing structural and dynamical information, J. Phys. Conf. Ser. (2012) 012010 IOP Publishing.
[91] M.G. Makowska, M. Strobl, E.M. Lauridsen, H.L. Frandsen, A. Tremsin, T. Shinohara, L.T. Kuhn, Phase transition mapping by means of neutron imaging in SOFC anode supports during reduction under applied stress, ECS Trans. 68 (2015) 1103–1114.
[92] M.G. Makowska, L.T. Kuhn, H.L. Frandsen, E.M. Lauridsen, S. De Angelis, L.N. Cleemann, M. Morgano, P. Trtik, M. Strobl, Coupling between creep and redox behavior in nickel-yttria stabilized zirconia observed in-situ by monochromatic neutron imaging, J. Power Sources 340 (2017) 167–175.
[93] N. Kardjilov, A. Hilger, I. Manke, R. Woracek, J. Banhart, CONRAD-2: the new neutron imaging instrument at the Helmholtz-Zentrum Berlin, J. Appl. Crystallogr. 49 (2016).
[94] M.G. Makowska, M. Strobl, E.M. Lauridsen, H.L. Frandsen, A.S. Tremsin, N. Kardjilov, I. Manke, J.F. Kelleher, L. Theil Kuhn, Effect of stress on NiO reduction in solid oxide fuel cells: a new application of energy-resolved neutron imaging, J. Appl. Crystallogr. 48 (2015) 401–408.
[95] A. Fedrigo, M. Strobl, A.R. Williams, K. Lefmann, P.E. Lindelof, L. Jørgensen, P. Pentz, D. Bausenwein, B. Schillinger, A. Kovyakh, Neutron imaging study of 'pattern-welded'swords from the Viking Age, Archaeol. Anthropol. Sci. (2016) 1–15.
[96] A.S. Tremsin, S.C. Vogel, M. Mocko, M.A.M. Bourke, V. Yuan, R.O. Nelson, D.W. Brown, W.B. Feller, Non-destructive studies of fuel pellets by neutron resonance absorption radiography and thermal neutron radiography, J. Nucl. Mater. 440 (2013) 633–646.
[97] S.C. Vogel, A review of neutron scattering applications to nuclear materials, ISRN Mater. Sci. 2013 (2013).
[98] H.-G. Brokmeier, W. Gan, C. Randau, M. Völler, J. Rebelo-Kornmeier, M. Hofmann, Texture analysis at neutron diffractometer STRESS-SPEC, Nucl. Instrum. Methods Phys. Res., Sect. A 642 (2011) 87–92.
[99] F. Malamud, J.R. Santisteban, V. Alvarez, R. Bolmaro, J. Kelleher, S. Kabra, W. Kockelmann, Texture analysis with a time-of-flight neutron strain scanner, J. Appl. Crystallogr. 47 (2014) 1337–1354.
[100] H. Bunge, P. Morris, Texture analysis in materials science: mathematical methods, 1982.
[101] M. Boin, R.C. Wimpory, A. Hilger, N. Kardjilov, S.Y. Zhang, M. Strobl, Monte Carlo simulations for the analysis of texture and strain measured with Bragg edge neutron transmission, J. Phys. Conf. Ser. 340 (2012) 012022.
[102] J. Santisteban, M. Vicente-Alvarez, P. Vizcaino, A. Banchik, S. Vogel, A. Tremsin, J. Vallerga, J. McPhate, E. Lehmann, W. Kockelmann, Texture imaging of zirconium based components by total neutron cross-section experiments, J. Nucl. Mater. 425 (2012) 218–227.
[103] H. Sato, T. Kamiyama, K. Iwase, T. Ishigaki, Y. Kiyanagi, Pulsed neutron spectroscopic imaging for crystallographic texture and microstructure, Nucl. Instrum. Methods Phys. Res., Sect. A 651 (2011) 216–220.
[104] H. Sato, O. Takada, K. Iwase, T. Kamiyama, Y. Kiyanagi, Imaging of a spatial distribution of preferred orientation of crystallites by pulsed neutron Bragg edge transmission, J. Phys. Conf. Ser. 251 (2010) 012070.
[105] H. Sato, T. Kamiyama, Y. Kiyanagi, A rietveld-type analysis code for pulsed neutron bragg-edge transmission imaging and quantitative evaluation of texture and microstructure of a welded. ALPHA.-Iron Plate, Mater. Trans. 52 (2011) 1294–1302.
[106] F. Kropff, J.R. Granada, R.E. Mayer, The bragg lineshapes in time-of-flight neutron powder spectroscopy, Nucl. Instrum. Methods Phys. Res. 198 (1982) 515–521.
[107] M. Boin, NXS: a program library for neutron cross section calculations, J. Appl. Crystallogr. 45 (2012) 603–607.
[108] T. Ungár, A. Borbély, The effect of dislocation contrast on x-ray line broadening: A new approach to line profile analysis, Appl. Phys. Lett. 69 (1996) 3173–3175.
[109] W. Woo, T. Ungár, Z. Feng, E. Kenik, B. Clausen, X-ray and neutron diffraction measurements of dislocation density and subgrain size in a friction-stir-welded aluminum alloy, Metall. Mater. Trans. A 41 (2010) 1210–1216.
[110] P. Scardi, M. Leoni, Whole powder pattern modelling, Acta Crystallogr. Sect. A: Found. Crystallogr. 58 (2002) 190–200.
[111] N. Kardjilov, I. Manke, A. Hilger, S. Williams, M. Strobl, R. Woracek, M. Boin, E. Lehmann, D. Penumadu, J. Banhart, Neutron Bragg-edge mapping of weld seams, Int. J. Mater. Res. 103 (2012) 151–154.
[112] L. Josic, A. Steuwer, E. Lehmann, Energy selective neutron radiography in material research, Appl. Phys. A 99 (2010) 515–522.
[113] L. Josic, E. Lehmann, A. Kaestner, Energy selective neutron imaging in solid state materials science, Nucl. Instrum. Methods Phys. Res., Sect. A 651 (2011) 166–170.
[114] N. Kardjilov, I. Manke, A. Hilger, S. Williams, M. Strobl, R. Woracek, M. Boin, E. Lehmann, D. Penumadu, J. Banhart, Neutron Bragg-edge mapping of weld seams, Int. J. Mater. Res. (2012) 151–154.
[115] M. Schulz, P. Böni, E. Calzada, M. Mühlbauer, B. Schillinger, Energy-dependent neutron imaging with a double crystal monochromator at the ANTARES facility at FRM II, Nucl. Instrum. Methods Phys. Res., Sect. A 605 (2009) 33–35.
[116] F. Salvemini, F. Grazzi, S. Peetermans, F. Civita, R. Franci, S. Hartmann, E. Lehmann, M. Zoppi, Quantitative characterization of Japanese ancient swords through energy-resolved neutron imaging, J. Anal. At. Spectrom. 27 (2012) 1494–1501.
[117] E. Lehmann, S. Peetermans, L. Josic, H. Leber, H. van Swygenhoven, Energy-selective neutron imaging with high spatial resolution and its impact on the study of crystalline-structured materials, Nucl. Instrum. Methods Phys. Res., Sect. A 735 (2014) 102–109.
[118] S. Peetermans, E. Lehmann, Simultaneous neutron transmission and diffraction contrast tomography as a non-destructive 3D method for bulk single crystal quality investigations, J. Appl. Phys. 114 (2013) 124905.
[119] W.D. Callister, D.G. Rethwisch, Materials Science and Engineering, John Wiley & Sons, NY, 2011.
[120] ASM, ASM Handbook Volume 9: Metallography and Microstructures, American Society For Metals, 2004.
[121] M. Strobl, N. Kardjilov, A. Hilger, D. Penumadu, I. Manke, Advanced neutron imaging methods with a potential to benefit from pulsed sources, Nucl. Instrum. Methods Phys. Res., Sect. A 651 (2011) 57–61.
[122] A.S. Tremsin, W. Kockelmann, A.M. Paradowska, Z. Shu-Yan, A.M. Korsunsky, T. Shinohara, W.B. Feller, E.H. Lehmann, Investigation of microstructure within metal welds by energy resolved neutron imaging, J. Phys. Conf. Ser. 746 (2016) 012040.
[123] R.R. Dehoff, M.M. Kirka, W.J. Sames, H. Bilheux, A.S. Tremsin, L.E. Lowe, S.S. Babu, Site specific control of crystallographic grain orientation through electron beam additive manufacturing, Mater. Sci. Technol. 31 (2015) 931–938.
[124] A. Tremsin, T. Yau, W. Kockelmann, Non-destructive examination of loads in regular and self-locking spiralock® threads through energy-resolved neutron imaging, Strain 52 (2016) 548–558.
[125] H.L. Frandsen, M. Makowska, F. Greco, C. Chatzichristodoulou, D. Ni, D. Curran, M. Strobl, L.T. Kuhn, P. Hendriksen, Accelerated creep in solid oxide fuel cell anode supports during reduction, J. Power Sources 323 (2016) 78–89.
[126] M.G. Makowska, M. Strobl, E.M. Lauridsen, S. Kabra, W. Kockelmann, A. Tremsin, H.L. Frandsen, L. Theil Kuhn, In situ time-of-flight neutron imaging of NiO–YSZ anode support reduction under influence of stress, J. Appl. Crystallogr. 49 (2016).

[127] M. Grosse, M. Steinbrueck, E. Lehmann, P. Vontobel, Kinetics of hydrogen absorption and release in zirconium alloys during steam oxidation, Oxid. Met. 70 (2008) 149–162.
[128] M. Grosse, G. Kuehne, M. Steinbrueck, E. Lehmann, J. Stuckert, P. Vontobel, Quantification of hydrogen uptake of steam-oxidized zirconium alloys by means of neutron radiography, J. Phys.: Condens. Matter 20 (2008) 104263.
[129] M. Große, E. Lehmann, M. Steinbrück, G. Kühne, J. Stuckert, Influence of oxide layer morphology on hydrogen concentration in tin and niobium containing zirconium alloys after high temperature steam oxidation, J. Nucl. Mater. 385 (2009) 339–345.
[130] L. Cai, K. An, Z. Feng, C. Liang, S.J. Harris, In-situ observation of inhomogeneous degradation in large format Li-ion cells by neutron diffraction, J. Power Sources 236 (2013) 163–168.
[131] L.G. Butler, B. Schillinger, K. Ham, T.A. Dobbins, P. Liu, J.J. Vajo, Neutron imaging of a commercial Li-ion battery during discharge: Application of monochromatic imaging and polychromatic dynamic tomography, Nucl. Instrum. Methods Phys. Res., Sect. A 651 (2011) 320–328.
[132] I. Manke, J. Banhart, A. Haibel, A. Rack, S. Zabler, N. Kardjilov, A. Hilger, A. Melzer, H. Riesemeier, In situ investigation of the discharge of alkaline Zn–Mn O 2 batteries with synchrotron x-ray and neutron tomographies, Appl. Phys. Lett. 90 (2007) 214102.
[133] H. Zhou, K. An, S. Allu, S. Pannala, J. Li, H.Z. Bilheux, S.K. Martha, J. Nanda, Probing multiscale transport and inhomogeneity in a lithium-ion pouch cell using in situ neutron methods, ACS Energy Lett. 1 (2016) 981–986.
[134] J.B. Siegel, X. Lin, A.G. Stefanopoulou, D.S. Hussey, D.L. Jacobson, D. Gorsich, Neutron imaging of lithium concentration in LFP Pouch cell battery, J. Electrochem. Soc. 158 (2011) A523–A529.
[135] K. Kino, M. Yonemura, Y. Ishikawa, T. Kamiyama, Two-dimensional imaging of charge/discharge by Bragg edge analysis of electrode materials for pulsed neutron-beam transmission spectra of a Li-ion battery, Solid State Ion. 288 (2016) 257–261.
[136] W.E. Frazier, Metal additive manufacturing: a review, J. Mater. Eng. Perform. 23 (2014) 1917–1928.
[137] D. Gu, W. Meiners, K. Wissenbach, R. Poprawe, Laser additive manufacturing of metallic components: materials, processes and mechanisms, Int. Mater. Rev. 57 (2012) 133–164.
[138] I. Gibson, D.W. Rosen, B. Stucker, Additive Manufacturing Technologies, Springer, 2010.
[139] W. Kockelmann, S. Siano, L. Bartoli, D. Visser, P. Hallebeek, R. Traum, R. Linke, M. Schreiner, A. Kirfel, Applications of TOF neutron diffraction in archaeometry, Appl. Phys. A 83 (2006) 175–182.
[140] N. Kardjilov, G. Festa, Neutron Methods for Archaeology and Cultural Heritage, Springer, 2016.
[141] S. Siano, L. Bartoli, J. Santisteban, W. Kockelmann, M. Daymond, M. Miccio, G. De Marinis, Non-destructive investigation of bronze artefacts from the marches national museum of archaeology using neutron diffraction, Archaeometry 48 (2006) 77–96.
[142] J.R. Santisteban, S. Siano, M.R. Daymond, Neutron strain scanning of archaeological bronzes, in: Materials Science Forum, Trans Tech Publ, 2006, pp. 975–980.
[143] K. Kino, N. Ayukawa, Y. Kiyanagi, T. Uchida, S. Uno, F. Grazzi, A. Scherillo, Analysis of crystallographic structure of a Japanese sword by the pulsed neutron transmission method, Physics Procedia 43 (2013) 360–364.
[144] Y. Kiyanagi, Y. Shiota, N. Ayukawa, K. Kino, T. Sato, H. Sato, H. Hasemi, T. Kamiyama, S. Uno, F. Grazzi, Anwendung einer transmissionsmethode mit gepulsten neutronen für eine studie zum kulturerbe, Restaurierung Archäologie 8 (2015) 85–91.
[145] N. Kardjilov, Recent developments at the CONRAD instrument at the Helmholtz Centre Berlin, in: Neutron Imaging User Symposium, Bad Zurzach, CH, 2012.
[146] N. Kardjilov, Neutron tomography in modern archaeology, Not.: Neutroni Luce Sincrotrone 13 (2008) 6–9.
[147] E. Barzagli, F. Grazzi, F. Salvemini, A. Scherillo, H. Sato, T. Shinohara, T. Kamiyama, Y. Kiyanagi, A. Tremsin, M. Zoppi, Wavelength resolved neutron transmission analysis to identify single crystal particles in historical metallurgy, Eur. Phys. J. Plus 129 (2014) 158.
[148] D.S. Hussey, C. Brocker, J.C. Cook, D.L. Jacobson, T.R. Gentile, W.C. Chen, E. Baltic, D.V. Baxter, J. Doskow, M. Arif, A new cold neutron imaging instrument at NIST, Physics Procedia 69 (2015) 48–54.
[149] N. Kardjilov, I. Manke, M. Strobl, A. Hilger, W. Treimer, M. Meissner, T. Krist, J. Banhart, Three-dimensional imaging of magnetic fields with polarized neutrons, Nat. Phys. 4 (2008) 399–403.
[150] W. Kockelmann, G. Burca, J.F. Kelleher, S. Kabra, S.-Y. Zhang, N.J. Rhodes, E.M. Schooneveld, J. Sykora, D.E. Pooley, J.B. Nightingale, F. Aliotta, R.C. Ponterio, G. Salvato, D. Tresoldi, C. Vasi, J.B. McPhate, A.S. Tremsin, Status of the neutron imaging and diffraction instrument IMAT, Physics Procedia 69 (2015) 71–78.
[151] Y. Kiyanagi, T. Shinohara, T. Kai, T. Kamiyama, H. Sato, K. Kino, K. Aizawa, M. Arai, M. Harada, K. Sakai, Present status of research on pulsed neutron imaging in Japan, Physics Procedia 43 (2013) 92–99.
[152] T. Shinohara, T. Kai, Commissioning start of energy-resolved neutron imaging system, RADEN in J-PARC, Neutron News 26 (2015) 11–14.
[153] H. Bilheux, K. Herwig, S. Keener, L. Davis, Overview of the conceptual design of the future VENUS neutron imaging beam line at the spallation neutron source, Physics Procedia 69 (2015) 55–59.
[154] M.G. Makowska, L. Theil Kuhn, L.N. Cleemann, E.M. Lauridsen, H.Z. Bilheux, J.J. Molaison, L.J. Santodonato, A.S. Tremsin, M. Grosse, M. Morgano, Flexible sample environment for high resolution neutron imaging at high temperatures in controlled atmosphere, Rev. Sci. Instrum. 86 (2015) 125109.
[155] D. Pooley, J. Lee, M. Brouard, R. Farrow, J. John, W. Kockelmann, R. Nickerson, N. Rhodes, E. Schooneveld, I. Sedgwick, 'GP2'—An energy resolved neutron imaging detector using a Gd coated CMOS sensor, in: Nuclear Science Symposium and Medical Imaging Conference (NSS/MIC), 2015 IEEE, IEEE, 2015, pp. 1–3.
[156] M. Morgano, E. Lehmann, M. Strobl, Detectors requirements for the ODIN beamline at ESS, Physics Procedia 69 (2015) 152–160.
[157] ProxiVision, http://www.proxivision.de/products/neutron-detector.html.